

# Number-conserving model for boson pairing

S. Fantoni

*International School for Advanced Studies, SISSA, I-34014 Trieste, Italy and  
International Centre for Theoretical Physics, ICTP, I-34014 Trieste, Italy*

T. M. Nguyen

*International Centre for Theoretical Physics, ICTP, I-34014 Trieste, Italy*

A. Sarsa

*International School for Advanced Studies, SISSA, I-34014 Trieste, Italy*

S. R. Shenoy

*International Centre for Theoretical Physics, ICTP, I-34014 Trieste, Italy*

(Dated: February 1, 2008)

An independent pair ansatz is developed for the many body wavefunction of dilute Bose systems. The pair correlation is optimized by minimizing the expectation value of the full hamiltonian (rather than the truncated Bogoliubov one) providing a rigorous energy upper bound. In contrast with the Jastrow model, hypernetted chain theory provides closed-form exactly solvable equations for the optimized pair correlation. The model involves both condensate and coherent pairing with number conservation and kinetic energy sum rules satisfied exactly and the compressibility sum rule obeyed at low density. We compute, for bulk boson matter at a given density and zero temperature, (i) the two-body distribution function, (ii) the energy per particle, (iii) the sound velocity, (iv) the chemical potential, (v) the momentum distribution and its condensate fraction and (vi) the pairing function, which quantifies the ODLRO resulting from the structural properties of the two-particle density matrix. The connections with the low-density expansion and Bogoliubov theory are analyzed at different density values, including the density and scattering length regime of interest of trapped-atoms Bose-Einstein condensates. Comparison with the available Diffusion Monte Carlo results is also made.

PACS numbers: 03.75.Fi, 05.30.Jp, 05.30.-d, 67.40.Db

## I. INTRODUCTION

Models for interacting bosons, a focus of interest for decades, have gained renewed importance due to the intense current activity in Bose-Einstein condensates [1, 2, 3, 4].

The Bogoliubov model for weakly interacting bosons [5, 6, 7] has long been the starting point for more detailed theories [8, 9, 10, 11, 12]. The ground state is approximated by an ideal Bose gas, and number conservation is violated by anomalous operator averages of the zero momentum condensate operator. Scattering out of (and depleting) the zero-momentum ground state produces opposite-momentum pairs that are treated as excitations with a linear spectrum [5].

Mean field pairing theories of superfluidity, by analogy with superconductivity, considered BCS-like anomalous pair-operator averages [10, 11], preventing an undesirable BCS gap in the excitation spectrum by a condition on the chemical potential [13]. When neutron scattering estimated that in He II, the condensate fraction was less than 10% [14, 15] while the superfluid fraction is 100%, such models were given added impetus, with pairing as a part (or whole) of the ground state. More detailed many-body ground state calculations based on Jastrow wavefunctions go beyond the simple mean-field pairing,

but to handle hard core potentials, must perforce have not only pairing, but also triplet, quadruplet and higher correlations. Thus many-body schemes like the hypernetted chain (HNC) approximation become open-ended hierarchies of coupled equations [7].

On the other hand, the discovery of Bose-Einstein condensate (BEC) with a finite number of atoms prompted investigation of number-conserving reformulations of the Bogoliubov model, without invoking anomalous averages, in modified Bogoliubov excitation operators [4, 16]. Although the BEC depletion fraction is estimated to be small, it is nonzero, and issues remain, of a generalized understanding of the 100% superfluid condensate [4].

Motivated by low carrier-density superconductivity in high  $T_c$  materials, negative- $U$  fermion pairing models have shown [17, 18] that *real space* pairing (as in pre-BCS models [9, 19]) occurs at low densities, and goes over to momentum space BCS pairing at high densities.

In this paper, we consider a non-Jastrow ground state of *number-conserving pairing* that ignores higher correlations, but includes *real space* pairing correlations *exactly*. What we lose in a description of normal-state correlations and densities close to crystallization, we gain in a focus on the correlations responsible for superfluidity at lower densities. The emergent picture is of superfluidity from *condensate plus real space pairs*, with the relative fraction dependent on density and interaction, but the

superfluid fraction always unity at  $T = 0$ . Within a pair-only model, the hypernetted chain scheme for the ground state *is now a closed form exactly soluble set of equations*, rather than being a correlation hierarchy, to determine the two-body distribution function and the density matrices. Numerical solution of the Euler equation, resulting from the Ritz variational principle, yields equation of states for any given soft-core potential, and a momentum distribution with the correct long wavelength behavior, having the proper Gavoret-Nozières singularity [20, 21].

Correlation functions show off diagonal long-range order (ODLRO), factoring into pairing functions that depend on the pair correlation defining the independent-pair ground state. Number conservation and other important sum rules are satisfied [7, 15, 21]. The Bogoliubov-type results are recovered not at low densities, but in the limit of large  $\rho a^3$ , where  $a$  is the interparticle scattering length.

The interaction-induced presence of nonzero-momentum particles yields an occupation number dependent wavevector that has some analogies with the ideal Fermi gas: one can define a nonzero *Bose wavevector*  $k_b$ , an average *Bose energy*  $E_b$ , and a corresponding *Bose temperature*  $T_b$ , that all vanish as a function of scaled density/interaction, i.e. in the ideal Bose gas limit.

More in detail, in this paper we use variational theory and Hyper Netted Chain methods [7, 22, 23] to add pair correlations to the mean field wave function, which is at the basis of the Gross-Pitaevsky approach. We consider the following ground state trial function which includes independent pair correlations (IPC) only

$$\begin{aligned} \Psi_{IPC}(\vec{r}_1, \dots, \vec{r}_N) = & 1 + \sum_{i < j} h(r_{ij}) \\ & + \frac{1}{2!} \sum_{(i < j) \neq (l < m)} h(r_{ij})h(r_{lm}) + \dots \end{aligned} \quad (1)$$

where the indices of the correlation factors  $h(r_{ij})$ , appearing in the above summed products, at all orders, never overlap. Writing  $h(r)$  in Fourier space, one can easily verify that with the IPC trial function of Eq. (1) the zero-momentum condensate fraction interconverts with *depletion* pairs with zero total momentum only. Note that  $h$  is real i.e. condensation phase is locked to coherent pairing phases. Thus the  $\Psi_{IPC}$  is characterized by a condensate and a coherent depletion.

Although this condensate plus pair (only) ansatz is in the broad spirit of the Bogoliubov model there are three crucial differences: i) Number conservation is maintained, with no anomalous averages; ii) The condensate and pairs are coherent and both are part of the ground state rather than the latter being excitations; iii) The expectation value of the *total* hamiltonian is evaluated, without truncation, so the energy is a rigorous upper bound, and the correlation  $h(r)$  obtained by minimiza-

tion goes beyond the Bogoliubov approximation. Excitations are not considered here, but will be related to density variations of the interaction-induced state of coherent condensate-pair interconversion.

The IPC model constitutes the underlying wave function of Coupled Cluster theory, in the SUB(2) approximation, which has been successfully used in a number of studies of strongly correlated systems [24, 25]. In comparison with the Jastrow ansatz,  $\Psi_J(R) = \prod_{i < j} (1 + h(r_{ij}))$ , the correlation products  $h(r_{ij})h(r_{lm}) \dots$  in Eq. (1) with  $(ij) \neq (lm)$  constitute only a subset of those produced by  $\Psi_J(R)$ , and, as a result,  $\Psi_{IPC}(R)$  cannot be put in a product form like  $\Psi_J(R)$ . Nonetheless,  $\Psi_{IPC}(R)$ , still satisfies the separability condition, namely for any  $\{R\} = \{R_1, R_2\}$   $\Psi_{IPC}(R_1, R_2) \rightarrow \Psi_{IPC}(R_1)\Psi_{IPC}(R_2)$ , in the limit of the subset of particles  $\{R_1\}$  being macroscopically far from  $\{R_2\}$ .

The trial function  $\Psi_{IPC}(R)$  of Eq. (1), not being of the product form, cannot deal directly with two-body potentials which have strong singularities at short distances, like the hard sphere potentials or those of the Lennard-Jones type. However, the detailed shape of the two-body potential may not be relevant for low-density systems, and suitable two-body pseudopotentials [26] can be found to study in a quantitative way the dynamical and superfluid properties of Bose systems.

We compute the two-body distribution function and one- and two-particle density matrices of a bulk boson system by using a new HNC cluster technique, based on the Renormalized Fermi Hyper Netted Chain (RFHNC) theory [23]. This new cluster technique is made necessary because of the particular form of  $\Psi_{IPC}(R)$ , which requires the summation of reducible and unlinked diagrams, contrary to the case of ordinary Jastrow theory. This novel method is based on treating the boson system as a collection of *Fermi particles*, having the same mass and interaction of the true bosonic ones, and a flavour degeneracy which equals the number of particles, so that they can all occupy the lowest state  $\vec{k} = 0$ . The above method relies on the property of the FHNC cluster expansion to be exact at any order in  $1/N$  [22, 23]. This could later permit the study of finite-atom trapped condensates.

The plan of this paper is as follows. In Section II, we present the diagrammatics of the hypernetted chain approximation, and show how the independent-pair model for the ground state allows for a closed set of equations. In Section III we relate the correlation functions (reduced or traced density matrix elements) to the pair correlation  $h(r)$  entering the ground state. In Section IV we derive the Euler equations for the *optimal*  $h(r)$  and the corresponding momentum distribution  $n(q)$ . Results for different soft-core potentials, and plots of various physical quantities are given in Section V. Finally, Section VI is a summary and conclusions.

## II. HNC THEORY FOR THE INDEPENDENT PAIR MODEL

We present in this Section the calculation of the two-body distribution function of a bulk boson system described by the IPC trial function of Eq. (1).

The pair distribution function  $g_2(1, 2)$  is one of the fundamental quantities in the study of interacting many-body systems. Both the structure function  $S(k)$  and the expectation value of the hamiltonian  $E[h]$  are given in terms of it. Therefore, its calculation is a necessary step for any quantitative analysis of the static and dynamical property of an interacting quantum many-body system. It is defined as

$$g_2(1, 2) = g(r_{12}) = \frac{N(N-1)}{\rho^2} \frac{\int d\vec{r}_3 d\vec{r}_4 \dots d\vec{r}_N |\Psi_{IPC}(R)|^2}{\int dR |\Psi_{IPC}(R)|^2} \quad (2)$$

where the first equality is due to the translational invariance of the system. The static structure function  $S(k)$  is strictly related to the pair function and given by [7]

$$S(k) = 1 + \rho \int d\vec{r} e^{i\vec{k} \cdot \vec{r}} (g(r) - 1) \quad (3)$$

The two-body distribution function  $g(r)$  satisfies the following normalization sum rule [7]

$$S(0) = 1 + \rho \int d\vec{r} (g(r) - 1) = 0 \quad (4)$$

### A. The new HNC scheme for the IPC model.

A new many-body method, based on the properties of the FHNC cluster expansion [22] and on the RFHNC summation technique [23], is developed and used in the calculation of  $g(r_{12})$ . We show below, as done in Ref. [23] for the Jastrow model, that RFHNC applied to N-flavour fermions (which are equivalent to a system of N bosons) produces the exact counting coefficients of the cluster diagrams in the independent pair ansatz.

The standard HNC cluster decomposition is based on (i) a series expansion of the r.h.s. of Eq. (2) around  $h(r) = 0$  and (ii) a diagrammatic representation of the various terms [45]. The independent pair condition in  $\Psi_{IPC}(R)$  implies that each vertex of any cluster diagram has at most two correlation lines reaching it, one coming from the ket  $|\Psi_{IPC}\rangle$  (K-correlation) and the other coming from the bra  $\langle\Psi_{IPC}|$  (B-correlation). This property, on the one hand, kills all the *Jastrow* elementary diagrams, but, on the other, leads to a highly non trivial cluster expansion with extra vertex corrections that can be summed. A new pairing-focussed HNC treatment,

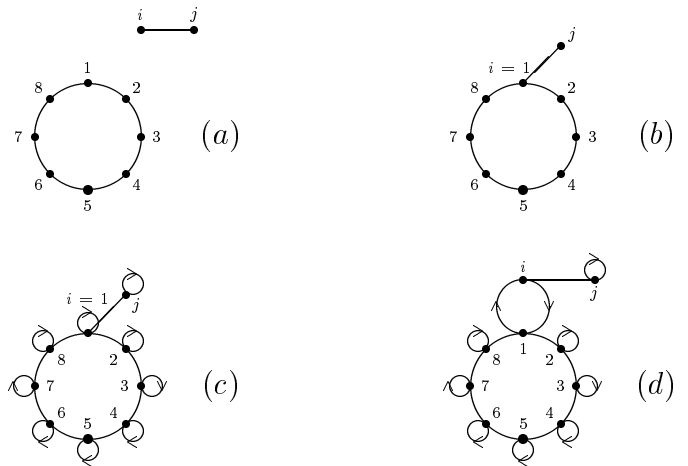


FIG. 1: Diagrams showing the cancellation process of the HNC and the FHNC cluster expansions as discussed in the text. All the four diagrams give the same cluster integral  $I$ , and are constituted by the two substructures  $\Gamma(1, \dots, s)$ , with  $s = 8$ , and  $\gamma(i, j)$ . Diagrams (a) and (b) are bosonic. Diagrams (c) and (d) are fermionic, and their oriented lines denote the exchange function  $l(k_F r)$ .

different from the standard one developed for Jastrow theory is needed to sum up the resulting cluster series, and (unlike Jastrow) it can be written in closed form.

A first important subdivision of the cluster diagrams is between *linked* and *unlinked* diagrams, where the unlinked diagrams are those with two or more non overlapping parts. The linked diagrams are further subdivided in *irreducible* and *reducible* diagrams. Reducible (or separable) diagrams correspond to cluster integrals which can be factorized in two or more parts.

In standard HNC, all the unlinked diagrams cancel each other, as schematically shown by the following simple example. The upper part of Fig. 1 displays two cluster diagrams, (1a) and (1b) from different terms of the Mayer expansion. Both are constituted with two linked diagrammatical structures,  $\Gamma(1, \dots, s)$  and  $\gamma(i, j) \equiv h(r_{ij})$ , where  $i$  or  $j$  may or may not coincide with one of the labels of  $\Gamma$ . The structure  $\Gamma(1, \dots, s)$  has  $s$  vertices, two of which correspond to the two *external* labels 1 and 2 of  $g(r_{12})$ ;  $\gamma(i, j)$  has two vertices only. Diagram (1a) is unlinked, whereas diagram (1b) is linked but reducible. Therefore, their corresponding cluster terms, in Figure 1, have the same integral form

$$I = \int d\vec{r}_1 \dots d\vec{r}_s \Gamma(\vec{r}_1, \dots, \vec{r}_s) \int d\vec{r}_i d\vec{r}_j \gamma(\vec{r}_i, \vec{r}_j). \quad (5)$$

The unlinked diagram (1a) comes from the unlinked term  $([\Gamma + \gamma])$  in the numerator of Eq. (2) or as a product  $([\Gamma \times \gamma])$  of the term  $(\Gamma)$  in the numerator and the term  $(\gamma)$  in the denominator. The reducible diagram (1b) comes from a numerator term. Let us now compute for each of them the counting coefficient due to the presence of

$\gamma(i, j)$ , under the assumption that the diagrammatical structure  $\gamma$  can be attached to any of the  $s$  vertices of  $\Gamma$  in diagram (1b) (as in the case of Jastrow theory) [46]

$$\begin{aligned} [\Gamma + \gamma]_a &\rightarrow + \frac{(N-s)(N-s-1)}{2\Omega^2}, \\ [\Gamma \times \gamma]_a &\rightarrow - \frac{N(N-1)}{2\Omega^2}, \\ [\Gamma + \gamma]_b &\rightarrow + \frac{s(N-s)}{\Omega^2}. \end{aligned} \quad (6)$$

Summing up the various coefficients, one can see that the leading terms (those in  $N^2/\Omega^2$ ) cancel out. Moreover, the next to leading order terms (those in  $N/\Omega^2$ ) also vanish. This means that the combined diagrammatic structures (1a) and (1b) do not contribute to the two-body distribution function in the thermodynamic limit. We have recovered in this example the well known property of the Mayer cluster expansion, that only irreducible diagrams contribute to  $g(r)$ , and the reducible and unlinked diagrams correspond to terms of order  $1/N$  or lower, which therefore vanish in the thermodynamic limit [47].

In the case of the IPC ansatz, not all the  $s$  reducible diagrams of type (1b) are allowed, as assumed in the previous equation. For instance, if a given vertex, amongst the  $s$  possible ones, has both a  $B$  and a  $K$  correlation reaching it in the  $\Gamma$  structure the second diagrammatical structure  $\gamma$  cannot be attached to it (so e.g. 1b can not occur). In this case, we do not have anymore the cancellation of the next to leading order terms and one has to include  $I$  of Eq. (5) (and, therefore both the unlinked and the reducible diagrams (1a) and (1b)) in the cluster expansion with the proper coefficient.

Let us now suppose that no reducible diagrams of the type (1b) are allowed. In this case, the leading coefficient of  $I$ , resulting from the sum of the contributions  $[\Gamma + \gamma]_a$  and  $[\Gamma \times \gamma]_a$  in Eq. (6), is proportional to  $N$  and given by  $-s\rho/\Omega$ . The translational invariance of  $\gamma$  brings in a factor  $\Omega$ , and the internal counting coefficient of  $\Gamma$  another factor  $t_\Gamma \times N(N-1) \dots (N-s+1)/\Omega^s$ , where  $t_\Gamma$  is the topological factor of  $\Gamma$  [48]. Therefore the total coefficient,  $\tilde{I}(\text{bosonic})$ , of the cluster term  $I$  is non-zero and given by

$$\tilde{I}(\text{bosonic}) = -t_\Gamma \times s\rho^{s+1}. \quad (7)$$

Unfortunately, the summation of reducible diagrams is very difficult in the general case, because it requires a direct counting of terms coming from the numerator and the denominator.

The situation is much simpler in the Fermi case, where one can use the FHNC cluster expansion. With fermions of  $\nu$  flavours, because of the Pauli principle, the various expansion terms in both the numerator and the denominator have coefficients, simply given by  $t \times (-)^{s+l} \rho^s / \nu^{s-l}$ , where  $t$  is a generic topological factor,  $s$  the number of

vertices,  $l$  the number of Pauli loops (counting also the one-vertex loops). As an example, the terms with no exchanges have only one-vertex loops, therefore  $s = l$ , and the coefficient is  $t \times \rho^s$ . The vertices in a Pauli loop are connected by the two-body Fermi function  $l(k_{Fr_{ij}})$ , given by

$$l(x) = \frac{3}{x^3}(\sin(x) - x\cos(x)), \quad (8)$$

where  $x = k_{Fr_{ij}}$  and  $k_F = (6\pi^2\rho/\nu)^{1/3}$  is the Fermi momentum.

One may easily verify that, given the structure of the coefficients of the cluster diagrams, there is a complete cancellation of the denominator with the unlinked terms of the numerator [22]. Therefore, referring to the example of Fig. 1, the corresponding *fermionic* diagrams of the cluster term  $I$  cannot be unlinked, as diagram (1a). The *fermionic* diagram corresponding to (1b) is diagram (1c), where Pauli one-vertex loops have been added up. The loops, however, do not change  $I$  because  $l(k_{Fr_{ii}}) = 1$ . Its global counting coefficient is  $t_\Gamma \times \rho^{s+1}$ .

In addition, there are other reducible *fermionic* diagrams, like diagram (1d), which have the same integral form of  $I$ . This is due to the normalization and completeness properties of the Fermi function  $l(k_{Fr_{ij}})$

$$\begin{aligned} \frac{\rho}{\nu} \int d\vec{r} l(k_{Fr}) &= \frac{\rho}{\nu} \int d\vec{r} l^2(k_{Fr}) = 1, \\ \frac{\rho}{\nu} \int d\vec{r}_3 l(k_{Fr_{12}}) l(k_{Fr_{32}}) &= l(k_{Fr_{12}}). \end{aligned} \quad (9)$$

It is well known that for the Jastrow-Slater model all the reducible diagrams of the two-body distribution function cancel out exactly, as for the Bose case [23]. One may understand such cancellation by looking at the two cluster structures (1c) and (1d). The coefficients of the two corresponding cluster terms are  $t_\Gamma \times s\rho^{s+1}$  for diagrams of type (1c) and  $-t_\Gamma \times s\rho^{s+1}/\nu$  for diagrams of type (1d) (the separability point in both the structures (1c) and (1d) can be any of the  $s$  vertices of  $\Gamma$ ). From the properties of the exchange function  $l(k_{Fr})$  given in eqs. (9), it follows that the two cluster terms cancel each other.

However for the IPC model, diagrams (1c) are not allowed for the same reason that (1b) is forbidden in the boson case (no B,K and  $\gamma$  lines from a single vertex). Hence one is left in the IPC/FHNC case with uncanceled diagrams of the (1d) type, and using loop integrals like 9 ends up in the cluster term  $I$  of Eq. (5) with a total coefficient

$$\tilde{I}(\text{fermionic}) = -t_\Gamma \times s\rho^{s+1}. \quad (10)$$

But this is exactly as in the case of bosonic diagrams (1a) and (1b): the FHNC result is the same as the HNC for bosons.

From the above discussion it follows that a convenient way to compute the two-body distribution function  $g(r_{12})$  of Eq. (2) is to consider a notional Fermi system, in which the fermions have the same mass of the original bosons, interact with the same potential, and have a flavour degeneracy equal to the number  $N$  of particles, so that they all occupy the lowest state with  $k = 0$ . We can then use the much simpler FHNC theory, under the constraint  $\nu = N$ , in a *bosonic* limit.

This  $\nu = N$  limit implies  $l(k_F r_{ij})/\nu \rightarrow 1/N$ . As a consequence, all the irreducible fermionic diagrams will vanish in the thermodynamic limit, except those having one vertex loop only, which coincide with the corresponding bosonic diagrams. The *reducible* fermionic diagrams survive, because integrations on the uncorrelated fermionic bonds bring  $\Omega$  factors. In the following, we will show how to calculate them in a simple and efficient way.

### B. Vertex corrections.

In order to include reducible diagrams we use RFHNC theory which treats irreducible *renormalized* diagrams characterized by vertex corrections for each of their vertices [23].

There are two kinds of vertex corrections

- *bosonic vertex correction*  $V_b$ . This vertex correction applies to vertices of type either  $B$  or  $K$ , which are reached only by *one*  $B$ - or  $K$ -correlation in the underlying irreducible structure;
- *fermionic vertex correction*  $V_f$ . This vertex correction applies to vertices of the type  $KB$ , namely those reached by *both*  $K$ - and  $B$ -correlations in the underlying irreducible structure, and, therefore they can be further reached by one Pauli loop.

The two  $k$ -independent vertex corrections  $V_b$  and  $V_f$  are inter-related and can be computed by using the RFHNC summation technique. The series of one-body diagrams corresponding to  $V_b$  is exemplified by Fig. 2 (a), whose sum is given by

$$V_b = V_b(K) = V_b(B) = \frac{\tilde{h}_0 V_f}{1 - \tilde{h}_0 V_f}, \quad (11)$$

where the Fourier transform  $\tilde{h}(k)$  of  $h(r)$  is defined as

$$\tilde{h}(k) = \rho \int d\vec{r} e^{i\vec{k} \cdot \vec{r}} h(r), \quad (12)$$

and  $\tilde{h}_0 \equiv \tilde{h}(k = 0)$ .

The vertex correction  $V_f$  concerns the reducible fermionic diagrams, which in the *boson* limit ( $\nu = N$ ) corresponds to *unlinked* bosonic diagrams (like diagram (1a)), with a coefficient given by the next to leading order in  $N$ .

A series of one-body diagrams contributing to  $V_f$  is displayed in Fig. 2 (b). The corresponding vertex correction  $S_1$  is given by

$$S_1 = 1 - 2V_b + 3V_b^2 - 4V_b^3 + \dots = \frac{1}{(1 + V_b)^2}. \quad (13)$$

Besides  $S_1$ , there is a second type of vertex correction,  $S_2$ , contributing to  $V_f$ . The diagrammatic representation of  $S_2$  is displayed in Fig. 2 (c), and is, explicitly

$$S_2 = \int \frac{d\vec{k}}{(2\pi)^3 \rho} \frac{\tilde{h}^2(k) V_f}{1 - \tilde{h}^2(k) V_f^2}. \quad (14)$$

The fermionic vertex correction  $V_f$  is made of vertices of the  $S_1$  and  $S_2$  type, as schematically shown in Fig. 2 (d), and it is given by

$$V_f = \frac{S_1}{1 + S_1 S_2} = \frac{1}{(1 + V_b)^2 + S_2}. \quad (15)$$

The vertex corrections  $V_b$  and  $V_f$  correctly satisfies the normalization condition for the one-body distribution function,  $g_1(1) = 1$ . The sum of the entire set of one-body diagrams is given by

$$g_1(1) = (1 + V_b)^2 V_f + S_2 V_f = 1. \quad (16)$$

### C. Pair distribution function.

The calculation of  $g(r_{12})$  can be done by using the FHNC summation technique for irreducible diagrams, renormalizing the vertices with the vertex corrections  $V_b$  and  $V_f$ , depending on the nature of the vertex itself. The independent pair nature of the trial function reduces the set of allowed cluster diagrams, and, as a consequence, the structure of the integral equations results to be quite different from that encountered in standard FHNC [23]. The pair distribution function is a sum of chain and composite diagrams.

The lowest order diagrams contributing to  $g(r_{12})$  are (i) the ideal Bose gas (uncorrelated) diagram,  $\Gamma_u(1, 2)$ , and the two-body correlated diagrams, either (ii) linear, or (iii) quadratic in  $h$ . They are displayed in Fig. 3, together with their expressions, which include vertex corrections. They correspond to the set of diagrams included in the lowest order constrained variational (LOCV) method [29], when the Jastrow correlation is taken of the form  $f(r) = 1 + V_f h(r)$  and the vertex correction  $(1 + V_b)^2 V_f$ , which gives the condensate fraction (see Eq. (29)), is set equal to 1.

The lowest order bond, used in the chain diagrams, is represented by the solid line and corresponds to the correlation function  $h(r)$ . After the inclusion of the vertex corrections, it gives the lowest order composite diagram

$$V_b = \text{---}\times\text{---} = \text{---}\bullet\text{---} + \text{---}\bullet\text{---}\bullet\text{---} + \dots \quad (a)$$

$$S_1 = \begin{array}{c} \times \\ | \\ \text{---}\bullet\text{---} \end{array} + \begin{array}{c} \times \quad \times \\ \diagdown \quad \diagup \\ \text{---}\bullet\text{---} \end{array} + \begin{array}{c} \times \quad \times \\ | \quad | \\ \text{---}\bullet\text{---}\bullet\text{---} \end{array} + \dots \quad (b)$$

$$S_2 = \text{---}\bullet\text{---}\bullet\text{---} + \text{---}\bullet\text{---}\bullet\text{---}\bullet\text{---} + \dots \quad (c)$$

$$V_f = \bullet = \text{---}\bullet\text{---} + \text{---}\bullet\text{---}\bullet\text{---}\bullet\text{---} + \dots \quad (d)$$

FIG. 2: Diagrammatic equations for the vertex corrections. Equation (a) gives the bosonic vertex correction  $V_b$ . Equations (b) and (c) refer to the vertex corrections  $S_1$  and  $S_2$  respectively. Equation (d) exemplifies the cluster series of the full fermionic vertex correction  $V_f$ . The solid lines represent the correlation function  $h(r)$ , whereas the oriented lines indicate the exchange function  $l(k_F r)$ .

$$\begin{array}{c} \bullet \\ 1 \end{array} \quad \begin{array}{c} \bullet \\ 2 \end{array} = 1$$

$$\begin{array}{c} B, K \\ \text{---}\bullet\text{---}\bullet\text{---} \\ 1 \quad 2 \end{array} = 2(1 + V_b)^2 V_f^2 h(r_{12})$$

$$\begin{array}{c} K \\ \text{---}\bullet\text{---}\bullet\text{---} \\ B \\ 1 \quad 2 \end{array} = V_f^2 h^2(r_{12})$$

FIG. 3: Vertex corrected two-body diagrams which contribute to the distribution function  $g(r_{12})$ , together with the expression of the corresponding cluster terms. The vertex corrections to the top diagrammatic structure  $\Gamma_u(1, 2)$  sum up to unity (see Eq. (16))

$$X_0(r_{12}) = 2(1 + V_b)^2 V_f^2 h(r_{12}). \quad (17)$$

There are four types of chain diagrams, depending on the nature ( $B, K$ ) of the external vertices. For symmetry reasons,  $N_{BK}(1, 2) = N_{KB}(2, 1) = N_{KB}(1, 2)$  and  $N_{BB}(1, 2) = N_{KK}(1, 2)$ . The allowed chain diagrams are only those constructed with the lowest order bond and they are given by

$$\begin{aligned} \tilde{N}_{BK}(q) &= \tilde{N}_{KB}(q) = (1 + V_b)^2 V_f \frac{\tilde{h}^2(q) V_f^2}{1 - \tilde{h}^2(q) V_f^2}, \\ \tilde{N}_{BB}(q) &= \tilde{N}_{KK}(q) = (1 + V_b)^2 V_f \frac{\tilde{h}^3(q) V_f^3}{1 - \tilde{h}^2(q) V_f^2}. \end{aligned} \quad (18)$$

The sum of all vertex corrected chain diagrams is

$$\begin{aligned} \tilde{N}(q) &= 2(1 + V_b)^2 V_f^2 (\tilde{N}_{BK}(q) + \tilde{N}_{BB}(q)) \\ &= 2(1 + V_b)^2 V_f \frac{\tilde{h}^2(q) V_f^2}{1 - \tilde{h}^2(q) V_f^2}. \end{aligned} \quad (19)$$

The vertex corrected composite diagrams contributing to  $g(r_{12})$  are given by

$$X(r_{12}) = X_0(r_{12}) + X_1(r_{12}) + X_2(r_{12}) , \quad (20)$$

where  $X_0(r)$  is given by Eq. (17) and the Fourier Transforms of  $X_1(r)$  and  $X_2(r)$  are

$$\begin{aligned} \tilde{X}_1(q) &= \left( \frac{\tilde{h}^2 V_f^2}{1 - \tilde{h}^2 V_f^2} \middle| \frac{\tilde{h}^2 V_f^2}{1 - \tilde{h}^2 V_f^2} \right)_q , \\ \tilde{X}_2(q) &= \left( \frac{\tilde{h} V_f}{1 - \tilde{h}^2 V_f^2} \middle| \frac{\tilde{h} V_f}{1 - \tilde{h}^2 V_f^2} \right)_q , \end{aligned} \quad (21)$$

where the convolution integral  $(\mid)_q$  is defined by

$$(f|g)_q \equiv \frac{1}{(2\pi)^2 \rho q} \int_0^\infty dp p f(p) \int_{|p-q|}^{p+q} dk k g(k) . \quad (22)$$

The sum of all the chain and composite diagrams gives the exact expression of the two-body distribution function  $g(r_{12})$  in the thermodynamic limit,

$$g(r_{12}) = 1 + N(r_{12}) + X(r_{12}) + O\left(\frac{1}{N}\right) , \quad (23)$$

The leading term of the  $O(1/N)$  terms is independent of the coordinate  $r_{12}$ , and has the form  $\alpha/N$ , where the constant  $\alpha$  is given by

$$\alpha = -1 - \rho \int d\vec{r}_{12} (N(r_{12}) + X(r_{12})) . \quad (24)$$

Notice that the constant  $\alpha/N$ , contributes to  $S(0)$ , and makes the normalization sum rule of Eq. (4) to be correctly satisfied, independently on the correlation function  $h(r)$  considered. The set of cluster diagrams giving  $\alpha$  is constituted by the renormalized two-body Pauli loop (the exchange of the uncorrelated diagram  $\Gamma_u(1,2)$  in Fig. 3) plus all those corresponding to its the convolution with  $g(r_{12}) - 1$ . Terms of the type  $f(r_{12})/N$  or higher order  $1/N$  terms can be easily calculated by using the proposed FHNC scheme, but they are not of interest for the present paper.

The static structure function can be easily calculated from Eq. (3), and it results to be

$$\begin{aligned} S(k) &= 1 + 2(1 + V_b)^2 V_f^2 \frac{\tilde{h}(k)}{1 - \tilde{h}(k) V_f} \\ &+ \left( \frac{\tilde{h}^2 V_f^2}{1 - \tilde{h}^2 V_f^2} \middle| \frac{\tilde{h}^2 V_f^2}{1 - \tilde{h}^2 V_f^2} \right)_k \\ &+ \left( \frac{\tilde{h} V_f}{1 - \tilde{h}^2 V_f^2} \middle| \frac{\tilde{h} V_f}{1 - \tilde{h}^2 V_f^2} \right)_k \\ &+ \frac{\alpha}{\Omega} \delta(k) . \end{aligned} \quad (25)$$

### III. DENSITY MATRICES.

We compute in this section the one- and two-body density matrices of a bulk boson system described by the IPC trial function. They give us important information, such as the condensate fraction, the (paired) depletion momentum distribution and the pairing function.

The one-body density matrix  $\rho_1(1, 1')$  is defined as

$$\begin{aligned} \rho(1, 1') &= \rho(r_{11'}) = \\ \Omega \frac{\int d\vec{r}_2 d\vec{r}_3 \dots d\vec{r}_N \Psi_{IPC}^*(1', 2, \dots, N) \Psi_{IPC}(1, 2, \dots, N)}{\int dR |\Psi_{IPC}(R)|^2} , \end{aligned} \quad (26)$$

and its related quantity, the one-particle momentum distribution is given by

$$\begin{aligned} n(k) &= \langle a_k^\dagger a_{\vec{k}} \rangle = \rho \int d\vec{r}_{11'} e^{i\vec{k} \cdot \vec{r}_{11'}} \rho(r_{11'}) \\ &= n_0 \delta(k) + n_d(k) , \end{aligned} \quad (27)$$

defining a condensate and boson-pair number distribution that can be independently evaluated in this IPC scheme. Notice that, with the above definitions, the momentum distribution normalization is a sum rule on  $n_0$  and  $n_d(k)$

$$\begin{aligned} 1 &= \int \frac{d\vec{k}}{(2\pi)^3 \rho} n(k) \\ &= n_0 + \int \frac{d\vec{k}}{(2\pi)^3 \rho} n_d(k) \end{aligned} \quad (28)$$

#### A. Condensate fraction and depletion contribution

The term independent of  $r_{11'}$  in the one-body density matrix, is the condensate fraction, and it is given by the product of the vertex corrections in the points 1 and 1' [28],

$$n_0 = \lim_{r_{11'} \rightarrow \infty} \rho(r_{11'}) = (1 + V_b)^2 V_f = \frac{(1 + V_b)^2}{(1 + V_b)^2 + S_2} \quad (29)$$

The coherent depletion term  $n_d(k)$  is given by a diagrammatic series characterized by chains of bonds, alternatively of the  $B$ - and the  $K$ -type, starting with the  $B$ -type from point 1 and reaching 1' with the  $K$ -type. Each vertex has a  $V_f$  correction (the external points 1 and 1' have a single vertex correction). The sum of this series is given by

$$n_d(k) = \frac{\tilde{h}^2(k) V_f^2}{1 - \tilde{h}^2(k) V_f^2} . \quad (30)$$

The normalization sum rule (28) is fully satisfied

$$\int \frac{d\vec{k}}{(2\pi)^3 \rho} n(k) = \frac{(1 + V_b)^2}{(1 + V_b)^2 + S_2} + S_2 V_f = 1, \quad (31)$$

and the depletion of the condensate is given by

$$1 - n_0 = S_2 V_f. \quad (32)$$

### B. ODLRO and pairing behaviour.

The study of the off-diagonal long range order and the calculation of the pairing function [30] are based upon the two-body density matrix, which is defined by

$$\rho_2(1, 2; 1', 2') = \frac{N(N-1)}{\rho^2} \quad (33)$$

$$\times \frac{\int d\vec{r}_3 d\vec{r}_4 \dots d\vec{r}_N \Psi^*(1', 2', 3, \dots, N) \Psi(1, 2, 3, \dots, N)}{\int dR |\Psi(R)|^2}.$$

The diagrammatical expansion of  $\rho_2(1, 2; 1', 2')$  is characterized by the four external vertices 1, 2, 1' and 2'. The particular form of the IPC wave function excludes the possibility that more than one  $h$ -bond reach any of these vertices. It follows that, in the thermodynamic limit, the three unlinked structures in Fig. 4 are the only ones which contribute to  $\rho_2$ , with the result

$$\begin{aligned} \rho_2(1, 2; 1', 2') &= \rho(1, 1')\rho(2, 2') \\ &+ n_0 (n_d(r_{12'}) + n_d(r_{1'2}) + P(r_{12}) + P(r_{1'2'})) \\ &+ P(r_{12})P(r_{1'2'}) + n_d(r_{12'})n_d(r_{1'2}) + O\left(\frac{1}{N}\right) \end{aligned} \quad (34)$$

where  $n_d(r)$  is the reverse-Fourier transform of the depletion momentum distribution  $n_d(k)$  of Eq. (30), and the function  $P(r)$ , defined by

$$n_0 P(r) = X_0(r) + N_{BB}(r) = X_0(r) + N_{KK}(r), \quad (35)$$

is the reverse-Fourier transform of the pairing function [30]

$$\tilde{P}(k) = \frac{\tilde{h}(k)V_f}{1 - \tilde{h}^2(k)V_f^2} = -\sqrt{n_d(k)(1 + n_d(k))}. \quad (36)$$

The three diagrammatical structures of Fig. 4 refer to direct terms of the cluster expansion of  $\rho_2$  of Eq. (33), namely those terms in which the coordinate 1 in  $\Psi$  corresponds to 1' in  $\Psi^*$ , and 2 to 2'. The corresponding *fermionic* diagrams have an exchange line joining 1 with 1' and another one joining 2 with 2', which are not drawn in the figure, and that, in the *bosonic* limit, tend to unity. The terms, in which 1 and 2 are exchanged are of order  $1/N$  or higher.

The various terms in Eq. (34) have been obtained as follows.

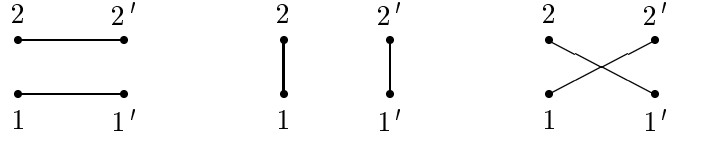


FIG. 4: Diagrammatical structures contributing to the two-particle density matrix. The four vertices of each structure are renormalized by their vertex corrections, as in Fig. 3. Each bond denotes either no correlations or a generic linked structure. The fully uncorrelated diagram should be counted only once.

- The first diagram on the left of Fig. 4 corresponds to the term  $\rho(1, 1')\rho(2, 2')$  in Eq. (34), which also includes the diagram with no bonds giving  $n_0^2$ .
- Diagrams belonging to the other two structures, having one bond only, contribute to terms of the type  $n_0 n_d$  and  $n_0 P$ . Those with two bonds give rise to the *pairing* and *anti-pairing* terms  $P \times P$  and  $n_d \times n_d$  respectively.
- By using the HNC theory developed in section 2, one can easily verify that the leading  $O(1/N)$  term of Eq. (34) is given by  $\alpha/N$ , exactly as for the two-body distribution function.

Simple inspection of Eq. (34) shows that the diagonal part of  $\rho_2(1, 2; 1', 2')$  coincides with the two-body distribution function  $g(r_{12})$ , namely

$$\rho_2(1, 2; 1, 2) = g(r_{12}). \quad (37)$$

The following independent-particle behaviour of the density matrix is found if the two particles 1 and 2 are far away from each other

$$\lim_{r_{12}, r_{1'2'} \rightarrow \infty} \rho_2(1, 2; 1', 2') = \rho(1, 1')\rho(2, 2'). \quad (38)$$

However, there is another interesting limit, which is associated with the ODLRO. This is when  $r$  and  $r'$  are far away from each other

$$\lim_{r_{11'}, r_{22'} \rightarrow \infty} \rho_2(1, 2; 1', 2') = (n_0 + P(r_{12}))(n_0 + P(r_{1'2'})), \quad (39)$$

indicating that the pairing function  $P(r)$  is related to the superfluidity properties of the boson model system [30, 33].

The two-particle momentum distribution  $n(\vec{k}_1, \vec{k}_2) = \langle a_{\vec{k}_1}^\dagger a_{\vec{k}_2}^\dagger a_{\vec{k}_1} a_{\vec{k}_2} \rangle$  can be computed by Fourier transforming the two-body density matrix [31, 32], namely

$$n_2(\vec{k}_1, \vec{k}_2) = \frac{\rho^2}{\Omega} \int d\vec{r}_{11'} d\vec{r}_{22'} d\vec{r}_{12} e^{i\vec{k}_1 \cdot \vec{r}_{11'} + i\vec{k}_2 \cdot \vec{r}_{22'}} \rho_2(1, 2; 1', 2'). \quad (40)$$



Eq. (37) guarantees that the normalization property

$$\int \frac{d\vec{k}_1 d\vec{k}_2}{(2\pi)^6 \rho^2} n_2(\vec{k}_1, \vec{k}_2) = (1 - \frac{1}{N}) , \quad (41)$$

is fully satisfied.

By inserting the r.h.s of Eq. (34) into Eq. (40), we get the result

$$\begin{aligned} n_2(\vec{k}_1, \vec{k}_2) &= n(k_1)n(k_2) + \\ &\frac{1}{\Omega} \left( \delta(\vec{k}_1)\delta(\vec{k}_2) \frac{2\rho n_0 \tilde{h}_0 V_f}{1 - \tilde{h}_0 V_f} + \delta(\vec{k}_1 + \vec{k}_2) \tilde{P}(k_1) \tilde{P}(k_2) \right. \\ &\left. + \delta(\vec{k}_1 - \vec{k}_2) n_d(k_1) n_d(k_2) + \delta(\vec{k}_1)\delta(\vec{k}_2) \alpha \rho \right) . \end{aligned} \quad (42)$$

Notice that the distribution of the  $(\vec{k}, -\vec{k})$  pairs results to be  $n_d(k)^2 + \tilde{P}(k)^2$ . This means that the distribution probability  $n_d^2(k)$  provided by a wave function with no ODLRO is increased by a finite amount given by  $\tilde{P}^2(k)$ . A similar feature is obtained for the  $(\vec{k}, \vec{k})$  pairs, whose distribution probability is increased by  $n_d^2(k)$ .

#### IV. ENERGY EXPECTATION VALUE AND EULER EQUATION.

The energy expectation value is defined as

$$E[h] = \frac{\langle V \rangle}{N} + \frac{\langle T \rangle}{N} . \quad (43)$$

The potential energy  $\langle V \rangle/N$  is given by

$$\begin{aligned} \frac{\langle V \rangle}{N} &= \frac{1}{2} \rho \int d\vec{r} v(r) g(r) \\ &= \frac{1}{2} \rho \int \frac{d\vec{q}}{(2\pi)^3 \rho} \tilde{v}(q) (S(q) - 1) + \frac{1}{2} \rho \int d\vec{r} v(r) , \end{aligned} \quad (44)$$

which can be computed by using either the expression for the pair function  $g(r)$  given in Eq. (23) or the static structure function of Eq. (25). Both  $g(r)$  and  $S(q)$  depend upon  $h(r)$ , therefore  $\langle V \rangle/N$  is a functional of  $h(r)$ .

The kinetic energy expectation value is defined as

$$\frac{\langle T \rangle}{N} = -\frac{\hbar^2}{2m} \frac{\langle \Psi | \nabla_1^2 | \Psi \rangle}{\langle \Psi | \Psi \rangle} , \quad (45)$$

The action of  $\nabla_1^2$  on  $\langle R | \Psi \rangle$  does not lead to three-body operators as in the Jastrow case, since

$$\begin{aligned} -\frac{\hbar^2}{2m} \nabla_1^2 \Psi(R) &= \sum_{i \neq 1} t(r_{1i}) \\ &+ \sum_{(i \neq 1) \neq (l \leq m)} t(r_{1i}) h(r_{lm}) + \dots \end{aligned} \quad (46)$$

where

$$\begin{aligned} t(r) &= -\frac{\hbar^2}{2m} \frac{1}{r} (h(r) r)'' , \\ \tilde{t}(q) &= \epsilon(q) \tilde{h}(q) , \end{aligned} \quad (47)$$

and  $\epsilon(q) = \hbar^2 q^2 / (2m)$  is the uncorrelated single particle energy.

The cluster expansion of  $\langle T \rangle/N$  is similar to that of the pair distribution function. The two-body diagram, with only one correlation line ( $t(r_{12})$ ) between the two external points 1 and 2, gives no contribution under  $r_{12}$ -integration. Therefore, one is left with the two-body correlated diagram, having both  $t(r_{12})$  and  $h(r_{12})$  as correlation lines, plus the composite diagrams given by  $t(r_{12})$  dressed by  $N_{LL}(r_{12})$  chains, leading to the following expression

$$\frac{\langle T \rangle}{N} = \int \frac{d\vec{q}}{(2\pi)^3 \rho} \frac{\tilde{t}(q) \tilde{h}(q) V_f^2}{1 - \tilde{h}^2(q) V_f^2} = \int \frac{d\vec{q}}{(2\pi)^3 \rho} \epsilon(q) n(q) . \quad (48)$$

The above equation proves that the kinetic energy sum rule is exactly satisfied in the IPC model with the FHNC treatment.

The total energy per particle  $E = \langle T \rangle/N + \langle V \rangle/N$  can be expressed in terms of the momentum distribution,

$$\begin{aligned} E[n_d] &= \int \frac{d\vec{q}}{(2\pi)^3 \rho} \epsilon(q) n_d(q) + \frac{1}{2} \tilde{v}(0) \\ &+ n_o \int \frac{d\vec{q}}{(2\pi)^3 \rho} (n_d(q) + \tilde{P}(q)) \tilde{v}(q) \\ &+ \frac{1}{2} \int \frac{d\vec{q}}{(2\pi)^3 \rho} \tilde{v}(q) (n_d | n_d)_q \\ &+ \frac{1}{2} \int \frac{d\vec{q}}{(2\pi)^3 \rho} \tilde{v}(q) (\tilde{P} | \tilde{P})_q . \end{aligned} \quad (49)$$

#### A. Applying the Ritz variational principle.

The Euler equation is obtained by applying the Ritz variational principle to the energy per particle  $E[h]$ .

$$\frac{\delta}{\delta \tilde{h}(q)} E[h] = 0 , \quad (50)$$

which gives rise to an integro-differential equation having  $\tilde{h}(q)$  as functional variable, derived in the Appendix.

Since the total energy can be expressed in terms of the background momentum distribution  $n_d(q)$  only, as shown in Eq. (49), then Eq. (50) can be written as

$$\frac{\delta E}{\delta \tilde{h}(q)} = \int dk \frac{\delta E}{\delta n_d(k)} \frac{\delta n_d(k)}{\delta \tilde{h}(q)} = 0 , \quad (51)$$

and from Eq. (49)

$$\begin{aligned} \frac{\delta E[n_d]}{\delta n_d(q)} &= \frac{q^2}{2\pi^2\rho} (\epsilon(q) \\ &+ n_0\tilde{v}(q) \left(1 - \frac{2n_d(q)+1}{2\sqrt{n_d(q)(1+n_d(q))}}\right) \\ &+ (\tilde{v}|n_d)_q - \frac{2n_d(q)+1}{2\sqrt{n_d(q)(1+n_d(q))}} (\tilde{v}|\tilde{P})_q \\ &- \int \frac{d\vec{k}}{(2\pi)^3\rho} \tilde{v}(k) (n_d(k) + \tilde{P}(k)) \Big) \end{aligned} \quad (52)$$

and the variation of  $n_d(q)$  with respect to  $\tilde{h}(k)$  is given by

$$\frac{\delta n_d(k)}{\delta \tilde{h}(q)} = 2V_f F(k) \delta(q-k) + \frac{\delta V_f}{\delta \tilde{h}(q)} 2\tilde{h}(k) F(k), \quad (53)$$

where the explicit expressions of the functions  $F(k)$  and  $\delta V_f/\delta \tilde{h}(q)$  can be found in the Appendix (see eqs. (A2) and (A1) respectively). Inserting Eq. (53) into Eq. (51), the Eq. (52) can be written as

$$\frac{\delta E[n_d]}{\delta n_d(k)} = \frac{k^2}{2\pi^2\rho} A[n_d], \quad (54)$$

where the  $k$ -independent term  $A[n_d]$  is given by

$$\begin{aligned} A[n_d] &= \frac{2}{V_f^2(a_1 + C)} \\ &\int_0^\infty dk n_d(k) \left(1 + n_d(k)\right) \times \frac{\delta E[n_d]}{\delta n_d(k)}, \end{aligned} \quad (55)$$

with the constants  $a_1$  and  $C$  defined in eqs. (A3) and (A2) respectively. Inserting the explicit expression of  $\delta E[n_d]/\delta n_d(k)$ , given in Eq. (52) into eqs. (54) and (55), we get the following system of integro-differential equations

$$\frac{2A}{V_f^2(a_1 + C)} \int \frac{d\vec{k}}{(2\pi)^3\rho} n_d(k) (1 + n_d(k)) = A, \quad (56)$$

where

$$\begin{aligned} A[n_d(q)] &= \epsilon(q) + n_0\tilde{v}(q) \left(1 - \frac{2n_d(q)+1}{2\sqrt{n_d(q)(1+n_d(q))}}\right) \\ &+ (\tilde{v}|n_d)_q - \frac{2n_d(q)+1}{2\sqrt{n_d(q)(1+n_d(q))}} (\tilde{v}|\tilde{P})_q \\ &- \int \frac{d\vec{k}}{(2\pi)^3\rho} \tilde{v}(k) (n_d(k) + \tilde{P}(k)) \end{aligned} \quad (57)$$

Going back to Eq. (51) we see that one optimal solution is  $A = 0$ . However, in Eq. (59) below we see that  $A$  may be non zero in order for the boson-pair number distribution  $n_d(k) \sim 1/k$  so the compressibility sum rule can be obeyed. Hence we consider only this solution.

## B. The IPC Euler equation

It is well known that the depletion component of the momentum distribution,  $n_d(q)$  has a  $1/q$  singularity in the long wavelength limit [20]. The behavior  $n_d(q) \rightarrow n_0 mc/(2q)$  at small  $q$ , where  $c$  is the sound velocity, uniquely depends upon the existence of a condensate and of a finite value of the compressibility [20, 21].

According to this important property, the long wavelength behavior of  $n_d(q)$  can be written as

$$n_d(q) \rightarrow \frac{d_{-1}}{q} + d_0 + d_1 q + \dots \quad \text{as} \quad q \rightarrow 0^+, \quad (58)$$

and, consequently,  $\tilde{h}(q)V_f \rightarrow -1 + q/(2d_{-1})$  as  $q \rightarrow 0$ . Using the above long wavelength behaviors, and developing the r.h.s. of Eq. (57) around  $q = 0$ , one gets the solution

$$A = -2 \int \frac{d\vec{k}}{(2\pi)^3\rho} \tilde{v}(k) \tilde{P}(k). \quad (59)$$

By substituting Eq. (59) in Eq. (57) one gets the following IPC Euler equation

$$\begin{aligned} \epsilon(q) + n_0\tilde{v}(q) \left(1 - \frac{2n_d(q)+1}{2\sqrt{n_d(q)(1+n_d(q))}}\right) \\ + (\tilde{v}|n)_q - \frac{2n_d(q)+1}{2\sqrt{n_d(q)(1+n_d(q))}} (\tilde{v}|\tilde{P})_q \\ - \int \frac{d\vec{k}}{(2\pi)^3\rho} \tilde{v}(k) (n_d(k) - \tilde{P}(k)) = 0, \end{aligned} \quad (60)$$

which is the a central result of the present paper. It is important to notice that the solution of Eq. (60), automatically satisfies Eq. (56). Substituting the expressions of  $a_1$  and  $C$  into Eq. (56), and using the long wavelength behavior  $\tilde{h}_0 V_f = -1$ , one gets

$$\int \frac{d\vec{k}}{(2\pi)^3\rho} n_d(k) = 1 + 2V_f \frac{\tilde{h}_0 V_f}{(1 - \tilde{h}_0 V_f)^3} = 1 - \frac{1}{4} V_f, \quad (61)$$

which can be used to express the vertex correction  $V_f$  in terms of the condensate fraction  $n_0$ ,

$$V_f = 4 \left(1 - \int \frac{d\vec{k}}{(2\pi)^3\rho} n_d(k)\right) = 4n_0. \quad (62)$$

The same results,  $V_b = 1/2$  and  $V_f = 4n_0$  follow from the vertex correction equations (11) and (15) and the depletion of the condensate given in Eq. (32).

Therefore, the IPC Euler equation (60) is consistent with the Gavoret–Nozières singularity for the long-wavelength behavior of the momentum distribution of a quantum Bose fluid.

The long wavelength behavior of the static structure function  $S(q)$ , resulting from the solution of the Euler equation (60) is given by

$$\begin{aligned} S(q) &\rightarrow S(0^+) + q \frac{dS(0^+)}{dq} \quad \text{as} \quad q \rightarrow 0^+, \\ S(0^+) &= 2 \int \frac{d\vec{k}}{(2\pi)^3 \rho} P^2(k) > 0. \end{aligned} \quad (63)$$

Notice that for the ideal Bose gas  $S(q) = S(0^+) = 1$ , whereas for the Jastrow ansatz, as well as for the exact

eigenfunction,  $S(0^+) = 0$ . Therefore, pair correlations alone are not sufficient to bring  $S(0^+)$  from one to zero. However, we will show that for the IPC model, and its Bogoliubov limit reasonable potentials yield  $S(0^+) \sim 0$ . Furthermore  $dS(q^+)/dq|_{q=0} \sim 1/(2mc)$ , namely the long wavelength behavior of  $S(q)$  is very close to that required by sum rules [21].

### C. Bogoliubov approximation

It is interesting to understand under which approximations our HNC theory recovers the Bogoliubov-type result. Since the sum of the chain diagrams corresponds to RPA theory, we expect that neglecting the composite diagrams  $X_1$  and  $X_2$  in the HNC summation lead to the Bogoliubov approximation [15]. Under this approximation, and setting the condensation fraction  $n_0 = 1$ , the total energy per particle of Eq. (49) is given by [6, 13]

$$\begin{aligned} E_{chain}[n_d] &= E_{un}[n_d] \\ &+ \int \frac{d\vec{q}}{(2\pi)^3 \rho} \left( \epsilon(q)n_d(q) + \tilde{v}(q) \left( n_d(q) - \sqrt{n_d(q) + n_d(q)^2} \right) \right), \end{aligned} \quad (64)$$

where

$$E_{un}[n_d] = \frac{1}{2} \tilde{v}(0), \quad (65)$$

is the energy upperbound obtained with the uncorrelated variational function  $\Psi(R) = 1$ .

Using Eq. (64) for the total energy, the Euler equation becomes

$$\epsilon(q) + \tilde{v}(q) \left( 1 - \frac{2n_d(q) + 1}{2\sqrt{n_d(q) + n_d(q)^2}} \right) = 0, \quad (66)$$

which yields the Bogoliubov solution for the momentum distribution

$$\begin{aligned} n_{Bog}(q) &= \frac{1}{2\omega(q)} (\epsilon(q) + \tilde{v}(q) - \omega(q)), \\ \omega^2(q) &\equiv \epsilon^2(q) + 2\epsilon(q)\tilde{v}(q). \end{aligned} \quad (67)$$

$n_{Bog}(q)$  goes as  $\sqrt{E_{un}}/(2q)$  in the long wavelength limit. This Bogoliubov momentum distribution function has been used as starting point in the numerical solution of the IPC Euler equation (60). Inserting  $n_{Bog}(q)$  back into Eq. (64) one recovers the Bogoliubov estimate for the total energy per particle

$$\begin{aligned} E_{Bog} &= \frac{1}{2} \tilde{v}(0) + \int \frac{d\vec{q}}{(2\pi)^3 \rho} (n_{Bog}(q) (\epsilon(q) + \tilde{v}(q)) \\ &- \tilde{v}(q) \sqrt{n_{Bog}(q) + n_{Bog}(q)^2}). \end{aligned} \quad (68)$$

The static structure function  $S_{Bog}(q)$  has a long wavelength behavior characterized by  $S(0^+) = 1 - n_0$  and  $dS(q)/dq|_{q=0^+} = n_0/(2\sqrt{E_{un}})$ .

The Bogoliubov approximation, and therefore our independent pair model, is best for those interactions such that the scattering length  $a$  coincides with its Born approximation

$$a_{\text{Born}} = \frac{m}{4\pi\hbar^2} \int d\vec{r} v(r) = \frac{m}{4\pi\rho\hbar^2} \tilde{v}(0). \quad (69)$$

Notice that  $a = a_{\text{Born}}$  in the case of a  $\delta$ -force interaction of the type  $v(r) = 4\pi\hbar^2 a \delta(\vec{r})/m$  [6]. For such an interaction, the Bogoliubov approximation coincides with the Lee and Yang [34] low-density expression

$$E_{LY} = \left( \frac{\hbar^2}{2ma^2} \right) 4\pi\rho a^3 \left[ 1 + \frac{128}{15} \sqrt{\frac{\rho a^3}{\pi}} \right], \quad (70)$$

and the momentum distribution goes as  $q^{-4}$  at large  $q$ .

TABLE I: Gaussian potentials used in the calculations of the weakly interacting Bose system. The strength  $v_0$  and the energy  $E_{un}$  of the uncorrelated system ( $\Psi(R) = 1$ ) are given in units  $\hbar^2/(2ma^2)$ . The width  $\sigma$  and the effective range  $r_{eff}$  are in units of the scattering length  $a$ .

Potential	$v_0$	$\sigma$	$a/a_B$	$r_{eff}$	$E_{un}/\rho$
G1	$1.1778 \times 10^{-3}$	11.256	0.95	-230.089	13.228
G2	$1.0028 \times 10^{-2}$	5.6127	0.90	-51.369	13.963
G3	$9.1978 \times 10^{-2}$	2.7887	0.80	-9.759	15.708

## V. RESULTS

In this section we present and discuss the results obtained for the equation of state, the two-body distribution function, the momentum distribution and the pairing function of a weakly interacting Bose system within the independent pair model, in correspondence with two different class of potentials.

For low density systems, like atomic vapours, of interest in the BEC physics, the only quantity which is considered to characterize the interaction is the scattering length  $a$ , namely its strength. For such systems,  $a \ll r_0$ , where  $r_0 = (3/(4\pi\rho))^{1/3}$  is the average distance between the particles. Recently, the possibility of creating Bose systems with relatively large values of  $\rho a^3$  has been opened up [35, 36]. For  $\rho a^3 > 10^{-4}$  the shape of the interaction becomes important for quantities such as the energy per particle and the condensate fraction [37].

In this paper we consider the properties of a Bose gas for  $\rho a^3$  in the range  $10^{-6} - 10^{-1}$ , or, equivalently for  $0.016 \leq (a/r_0) \leq 0.75$ . The pseudo-potentials  $v(r)$  used are purely repulsive and have a range of interaction which goes from  $\sim 0.1r_0$  to  $\sim 10r_0$ . We have considered two different choices for  $v(r)$

(i) Repulsive gaussian (G) potential defined by

$$v(r) = v_0 e^{-\frac{r^2}{2\sigma^2}}, \quad (71)$$

where  $\sigma$  is the width of the gaussian. Table I gives the values of the parameters  $v_0$  and  $\sigma$  of three different choices of gaussian potentials, labelled with G1, G2 and G3.

(ii) Soft-sphere (SS) potential defined by

$$v(r) = \begin{cases} v_0 & \text{if } r \leq R, \\ 0 & \text{otherwise,} \end{cases} \quad (72)$$

where we have taken  $R = 5a$  and  $R = 10a$  as in [37]. The values of the parameters are reported in Table II.

Tables I and II give also the effective range parameter  $r_{eff}$ , the ratio  $a/a_{Born}$  and the energy upperbound

TABLE II: Soft-sphere potentials used in the calculations of the weakly interacting Bose system and taken from Ref. [37]. The strength  $v_0$  and the energy  $E_{un}$  of the uncorrelated system ( $\Psi(R) = 1$ ) are given in units  $\hbar^2/(2ma^2)$ . The range parameter  $R$  and the effective range  $r_{eff}$  are in units of the scattering length  $a$ .

Potential	$v_0$	$R$	$a/a_B$	$r_{eff}$	$E_{un}/\rho$
SS10	$6.8167 \times 10^{-3}$	10	0.880	-29.936	14.280
SS5	$6.3086 \times 10^{-2}$	5	0.761	-4.9637	16.513

TABLE III: Energy per particle of the IPC model divided by the density,  $E_{IPC}/\rho$ , at various densities, for the five potentials considered. The IPC upperbounds are compared with the low-density expansion estimates of Eq. (70). The energies are given in units of  $\hbar^2/(2ma^2)$  and the density  $\rho$  in  $a^{-3}$ . In these units  $E_{LY0}/\rho = 4\pi = 12.556$

$\rho$	$E_{LY}/\rho$	G1	G2	G3	SS10	SS5
$10^{-6}$	12.63	12.63	12.63	12.64	12.65	12.68
$10^{-5}$	12.76	12.73	12.76	12.80	12.78	12.85
$10^{-4}$	13.17	12.92	13.05	13.22	13.11	13.31
$10^{-3}$	14.48	13.11	13.48	14.06	13.64	14.31
$10^{-2}$	18.62	13.20	13.81	15.01	14.08	15.56
$10^{-1}$	31.70	13.22	13.93	15.55	14.24	16.33

$E_{un}$  provided by the uncorrelated (ideal) Bose gas. The scattering length  $a$  has been calculated by using a standard procedures [38]. Notice in the case of a delta-type potential, when  $a/a_{Born} = 1$  and  $E_{Bog} = E_{LY}$ , the upperbound  $E_{un}$  coincides with the lowest order term of the Lee and Yang expansion,  $E_{LY0} = (\hbar^2/(2ma^2))4\pi\rho a^3$ .  $E_{LY0}$  has been proved to be an energy lower bound in the limit of  $\rho a^3 \rightarrow 0$  and under general conditions of the interaction, which are met by the potentials considered here [39].

The Euler equation (60) has been solved numerically by means of a self-consistent iterative procedure. Few iterations were sufficient to reach convergence for all the cases considered. The *optimal*  $n_d(q)$  has been found to have the  $n_0 mc/(2q)$  behavior in the long wavelength limit. The results for the IPC energy per particle of Eq. (49) are displayed in Table III in correspondence with the five potentials considered, and in Figs. 5 and 6 for the soft-sphere potentials.  $E_{IPC}$  can be compared with the upperbounds provided by  $E_{un}$  of Eq. (65), given in Tables I and II and the estimates from the low density expansion,  $E_{LY}$ , of Eq. (70), which are independent on the shape of the potential. Figs. 5 and 6 compare the IPC results with  $E_{Bog}$  of Eq. (68) and with the available DMC calculations [37]. The figures display also the DMC [37] and Jastrow [40] results for the hard-sphere potential.

The above results deserve the following comments

(i) the IPC upperbounds are above the Bogoliubov estimates for all the pseudopotentials and the density values considered. Therefore, the terms of the

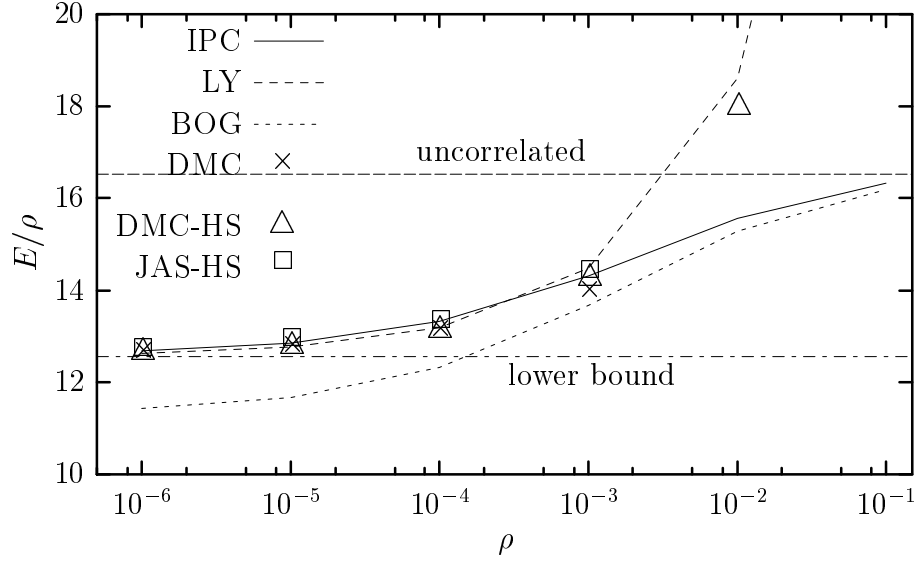


FIG. 5: Energy per particle or equation of state of a weakly interacting Bose gas for the soft-sphere potential SS5. The IPC results (solid line) are compared with the low density estimates  $E_{LY}$  (dashed line), those coming from the Bogoliubov approximation (dotted line),  $E_{Bog}$ , and the DMC calculations of Ref. [37] (crosses). The DMC [37] (triangles) and Jastrow [40] (squares) results obtained in correspondence with the hard-sphere potential are also reported for completeness. The energies are in units of  $\hbar^2/(2ma^2)$ , and the density  $\rho$  in units of  $a^{-3}$ .

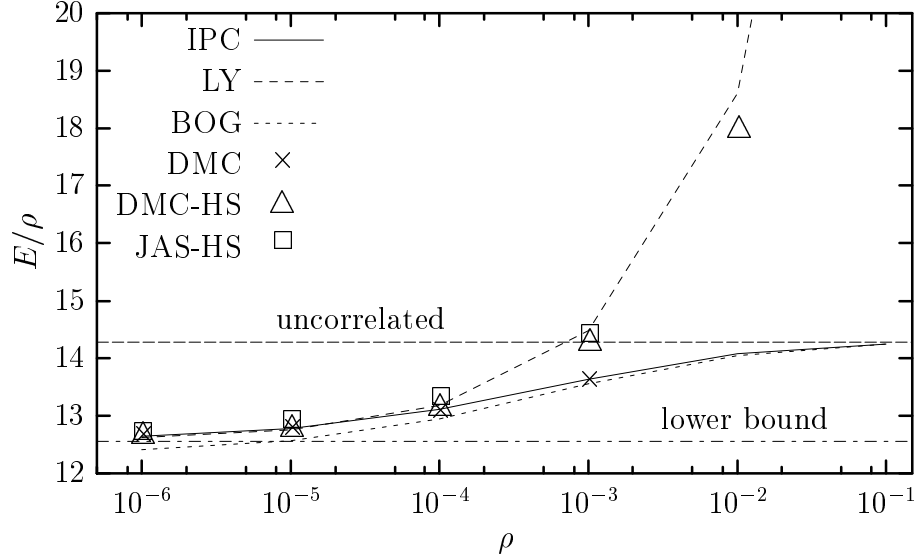


FIG. 6: Energy per particle or equation of state of a weakly interacting Bose gas for the soft-sphere potential SS10. The IPC results (solid line) are compared with the low density estimates  $E_{LY}$  (dashed line), those coming from the Bogoliubov approximation (dotted line),  $E_{Bog}$ , and the DMC calculations of Ref. [37] (crosses). The DMC [37] (triangles) and Jastrow [40] (squares) results obtained in correspondence with the hard-sphere potential are also reported for completeness. The energies are in units of  $\hbar^2/(2ma^2)$ , and the density  $\rho$  in units of  $a^{-3}$ .

hamiltonian neglected in Bogoliubov theory give a repulsive contribution. Notice that, contrary to  $E_{IPC}$ ,  $E_{Bog}$  is not an energy upperbound. The relative differences between the IPC and Bogoliubov results,  $(E_{IPC} - E_{Bog})/E_{Bog}$ , are reported on Table IV. One can see that  $E_{IPC}$  and  $E_{Bog}$  get closer and closer when either  $a/a_{Born} \rightarrow 1$  or for increas-

ing values of  $\rho a^3$ . In these two limits they both approach  $E_{un}$  from below.

- (ii) the low density expression of Eq. (70) starts failing already at  $\rho a^3 \sim 10^{-3}$ . At this density value and above it  $E_{LY}$  is always larger than  $E_{IPC}$ . The next to leading order in the low density expansion, giving a term in  $\rho^2 \log(\rho)$  [41], improves the total

TABLE IV: Comparison between the IPC model and the Bogoliubov theory. The table reports the relative difference  $\frac{E_{IPC} - E_{Bog}}{E_{Bog}} \times 10^3$  for the five potentials considered. The density is given in units of  $a^{-3}$ .

$\rho$	G1	G2	G3	SS10	SS5
$10^{-6}$	2.589	12.34	68.05	19.11	109.6
$10^{-5}$	2.053	10.80	62.62	17.03	101.4
$10^{-4}$	1.143	7.541	49.54	12.51	81.32
$10^{-3}$	0.355	3.353	28.19	6.337	47.82
$10^{-2}$	0.063	0.836	9.934	2.451	18.43
$10^{-1}$	0.010	0.163	2.713	0.276	9.003

energy estimates up to  $\rho a^3 \sim 10^{-4}$  (adding this correction term to  $E_{LY}$  the low density expansion agrees with DMC [37] within three digits). However, it gives too much attraction at higher density values. For instance, in the units of Fig. 5, the correction at  $\rho a^3 = 10^{-3}$  is  $-1.706$ , and at  $\rho a^3 = 10^{-2}$  is  $-11.37$ .

- (iii) there is an overall agreement of the IPC upper-bounds with the available DMC [37] results, even for the SS5 potential, which is the one with the shorter range of interaction. Contrary to  $E_{LY}$  and to  $E_{Bog}$ , both the IPC and DMC results are sandwiched between  $E_{un}$  and the lower bound  $E_{LY0}$  in the full range of density values considered.
- (iv) the shape of the potential starts becoming important already at  $\rho a^3 \sim 10^{-4}$ . Therefore, in the region of large  $a$ , the scattering length is not anymore sufficient to determine the interaction.

The condensate fraction  $n_0$  is displayed in Fig. 7 for the potentials G1, G3 and SS5 as a function of  $\rho a^3$ , and compared with the low-density expansion [5, 6, 42]

$$n_0 = 1 - \frac{8}{3} \sqrt{\frac{\rho a^3}{\pi}}. \quad (73)$$

One can see that the condensate fraction of the IPC model starts flattening at  $\rho a^3 \approx 10^{-2}$ , as for the case of  $E/\rho$ . However, it remains below one up to the highest density value considered.

The depletion momentum distribution  $n_d(k)$  for the potential SS10 at three density values is displayed in Fig. 8. The optimized distribution has interaction induced  $k \neq 0$  (pair) occupation even at  $T = 0$ , reminiscent of the Fermi distribution.

Following the Fermi analogue it is useful to formally define Bose wavevector  $q_b$  and bose energy,  $\epsilon_d$  and temperature  $T_b$  through

$$n_d(q_b) \equiv \frac{1}{2}, \quad \epsilon_d \equiv \frac{\hbar^2 q_b^2}{2m} \equiv k_B T_b \quad (74)$$

The arrows in Fig. 8 denote the bose wavevectors for the densities considered. For the typical values of the scattering length and mean interparticle spacing, 50 Å and 2000 Å respectively, typical of BEC [4], we find that  $\epsilon_p \approx 1.1210^{-11}$  eV and  $T_b \approx 0.134 \mu$  K.

To better show the  $q^{-1}$  behavior in the long wavelength limit, the figure plots  $q n_d(q)$  rather than  $n_d(q)$ . Similar results have been obtained for the other four potentials. The extrapolated values at  $q \rightarrow 0$  are compared with the theoretical sum rule value  $d_{-1}^{SR} = \sqrt{n_0^2 \mathcal{K}/4}$  where the compressibility  $\mathcal{K}$  is given by

$$\mathcal{K} = \frac{d}{d\rho} \left( \rho^2 \frac{dE}{d\rho} \right) = mc^2, \quad (75)$$

We plot in Fig. 9 the quantity

$$\Delta = \frac{d_{-1}}{d_{-1}^{SR}} \quad (76)$$

as a function of  $\rho a^3$  for the potentials G1, G3 and SS5. The compressibility sum rule is satisfied when  $\Delta = 1$ . For the sake of clarity we also plot in the lower panel the following difference function

$$\delta n_d(q) = n_d(q) - \frac{d_{-1}^{SR}}{q}. \quad (77)$$

We have found that over a range of densities  $\rho a^3 \lesssim 10^{-3}$  the compressibility sum rule is satisfied within three significant figures.

The coefficient  $d_{-1}$  can also be calculated directly, by using the following expression, which results from the terms in  $q^{-1}$  of the Euler equation (60).

$$d_{-1}^2 = \frac{n_0 \tilde{v}_0 + \int \frac{d\tilde{q}}{(2\pi)^3 \rho} \tilde{v}(q) \tilde{P}(q)}{8 \left( 1 + \frac{1}{6} \int \frac{d\tilde{q}}{(2\pi)^3 \rho} \left( n_d(q) - \tilde{P}(q) \right) \nabla_q^2 \tilde{v}(q) \right)}. \quad (78)$$

The coefficient  $d_{-1}$  obtained from the above equation and  $\lim_{q \rightarrow 0} q n_d(q)$  coincide within three digits for all the cases considered in the present calculation.

We have also computed the chemical potential defined by

$$\mu = E + \rho \frac{dE}{d\rho}. \quad (79)$$

The results obtained for the sound velocity and for the chemical potential are given in Table V for the potential G1, which has the ratio  $a/a_{\text{Born}}$  closer to 1. The corresponding estimates resulting from the low density expansion of Eq. (70), and given by

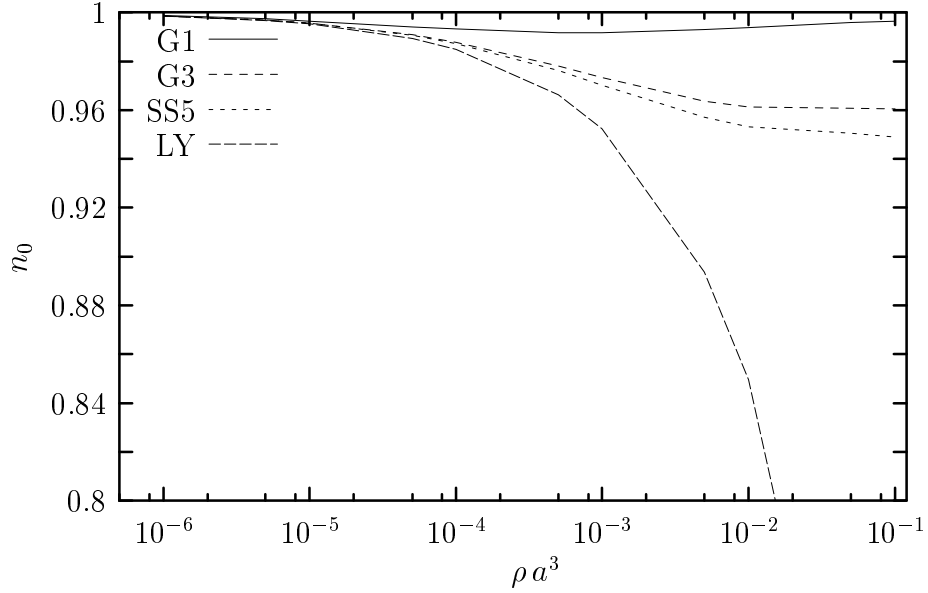


FIG. 7: Condensate fraction of a weakly interacting Bose gas as a function of the density for the potentials G1, G3 and SS5. The low density expression of Eq. (73) is also reported for comparison.

TABLE V: Sound velocity  $c$  and chemical potential  $\mu$  at various density values for the potential G1. The low-density results given in eqs. (81) are also reported for comparison. The density is given in units of  $a^{-3}$  and the compressibility,  $mc^2$ , and chemical potential,  $\mu$ , in units of  $\hbar^2/(2ma^2)$

$\rho$	$(mc^2/\rho)_{LY}$	$(mc^2/\rho)_{IPC}$	$(\mu/\rho)_{LY}$	$(\mu/\rho)_{IPC}$
$10^{-6}$	25.36	25.35	25.28	25.28
$10^{-5}$	25.85	25.67	25.61	25.52
$10^{-4}$	27.40	26.11	26.65	25.92
$10^{-3}$	32.31	26.39	29.92	26.28
$10^{-2}$	47.82	26.45	40.26	26.42
$10^{-1}$	96.88	26.46	72.96	26.45

$$(mc^2)_{LY} = \left( \frac{\hbar^2}{2ma^2} \right) 8\pi\rho a^3 \left( 1 + 16\sqrt{\frac{\rho a^3}{\pi}} \right), \quad (80)$$

$$(\mu)_{LY} = \left( \frac{\hbar^2}{2ma^2} \right) 8\pi\rho a^3 \left( 1 + \frac{32}{3}\sqrt{\frac{\rho a^3}{\pi}} \right), \quad (81)$$

are also reported in the table.

The pair correlation function  $h(r)$  multiplied by the vertex correction  $V_f$  can be calculated from the momentum distribution  $n_d(q)$ , by using Eq. (30). Its Fourier transform is plotted versus  $q$  in Fig. 10 at three different values of  $\rho a^3$  for the potential SS10.

Finally, the two-body distribution function  $g(r_{12})$  and the pairing function  $P(r_{12})$  are displayed in Figs. 11 and 12 respectively, for the case of the potential SS10. Similar plots can be shown for the other potentials. The long wavelength limits of the static structure function,  $S(0^+)$ , obtained in correspondence with the  $g(r_{12})$  reported in

Fig 11 are small, 0.0102, 0.0270 and 0.0551 for  $\rho a^3 = 10^{-5}, 10^{-4}, 10^{-3}$  respectively. The values extrapolated directly from  $S(q)$  and those computed from Eq. (63) coincide within three digits for all the cases considered.

The pairing function  $P(r_{12})$ , as the one-body density matrix  $\rho(r_{11'})$ , is long-ranged. Its Fourier transform,  $\tilde{P}(q)$ , has therefore a singular long wavelength behavior, given by  $-n_0 mc/(2q)$ , opposite to that of the momentum distribution  $n_d(q)$ . Therefore, the function  $F_1(r) = P(r) + \rho(r)$  is a short-range function. This function is the key ingredient of the following important ODLRO property of the semi-diagonal two-body density matrix [21, 43]

$$\lim_{r' \rightarrow \infty} \rho(1, 2; 1', 2) = n_0(1 + F_1(r_{12})). \quad (82)$$

One can easily verify that  $\tilde{F}_1(0) = -1/2$ , as required by the Stringari sum rule on the two-body density matrix [21]. Such a behavior of  $\tilde{F}_1(q)$  has important consequences on the overlap between the particle and density excited states [44]. Moreover the sum rule relating  $\mu$  to  $F_1$  [21] is satisfied numerically to three significant figures [44] implying gapless excitation.

## VI. CONCLUSIONS AND PERSPECTIVES

In this paper we have used the variational theory to develop a number-conserving model for boson pairing based upon the Bogoliubov theory. This model considers an independent pair correlated wave function as trial function, which is characterized by a 100% condensation of  $(\vec{k}, -\vec{k})$  pairs.

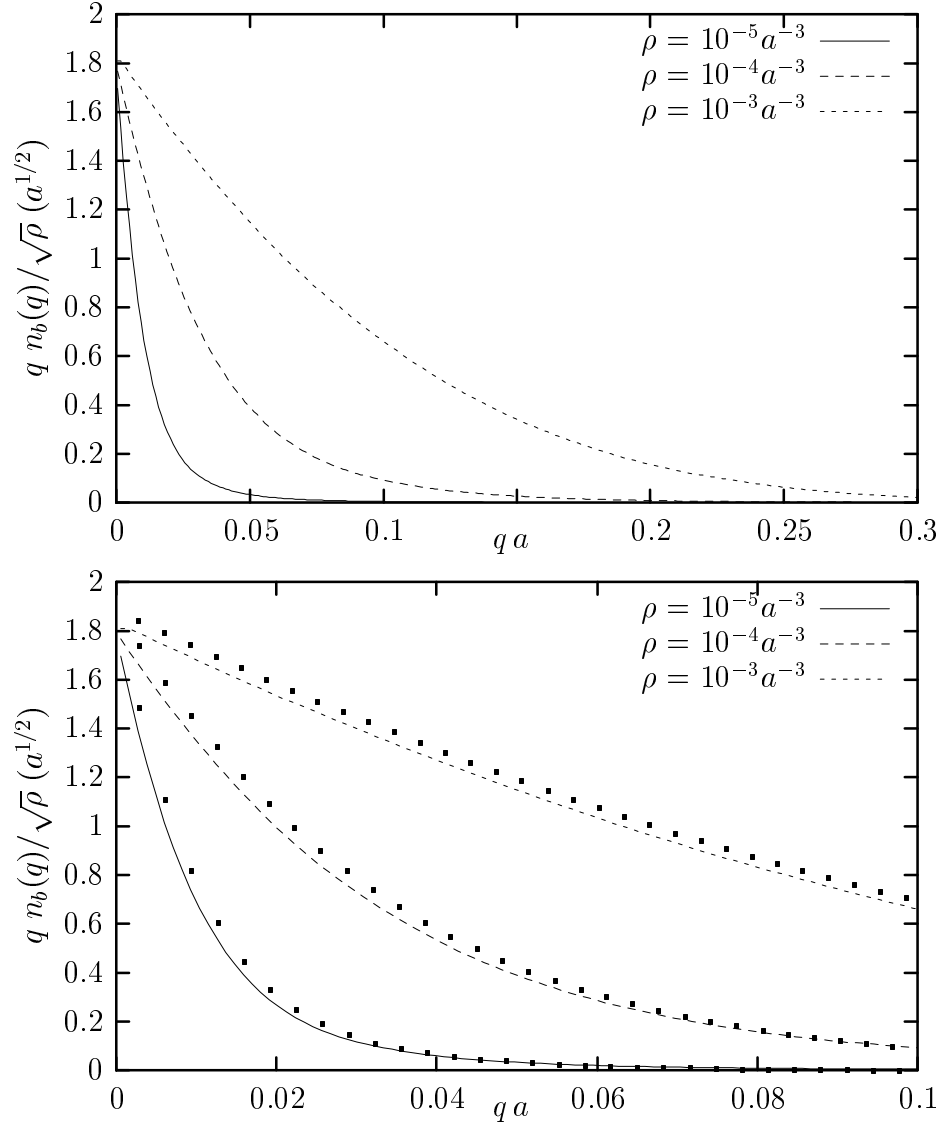


FIG. 8: Momentum distribution of the IPC model of a Bose gas interacting with the potential SS10 at several densities. The momentum distribution  $n_d(q)$  is multiplied by  $q$  to make clear the  $q^{-1}$  long wavelength behavior and divided by  $\sqrt{\rho}$  to fit the scale. The full circles in the lower panel indicate the Bogoliubov results,  $\sqrt{E_{un}}/2$ .

The cluster expansions for the two-body distribution function  $g(r_{12})$  and the one- and two-body density matrices from the IPC trial function have been derived, and a scheme of the HNC type has been developed to sum up the cluster terms to all order in a fully closed form. This novel HNC method maps the Bose system into a Fermi system, such that the fermions have as many flavours as the number of particles, and then it makes use of the Renormalized FHNC theory to compute the resulting cluster terms.

As a consequence, the energy expectation value can be obtained with no approximation for any given pair correlation  $h(r)$ , resulting in a true energy upperbound. Similarly, the normalization sum rules on  $g(r_{12})$ ,  $\rho(r_{11'})$  and  $\rho_2(1, 2; 1', 2')$ , as well as the kinetic energy sum rule,

are exactly satisfied. This cannot be achieved in Jastrow theory, where truncations of the cluster series are intrinsically made.

The Euler equation to get the optimal pair correlation  $h(r)$ , obtained in accordance with the Ritz variational principle, has been derived. Since the total energy per particle can be written in terms of the momentum distribution only, we could derive the integro-differential equation having the momentum distribution as variable, instead of  $h(r)$ . We found that the Euler equation in  $n_d(q)$  is not uniquely determined, and we selected the one consistent with a momentum distribution which has the Gavoret-Nozières singularity in the long wavelength limit. We proved that such an Euler equation can be numerically solved by means of a rather simple iterative



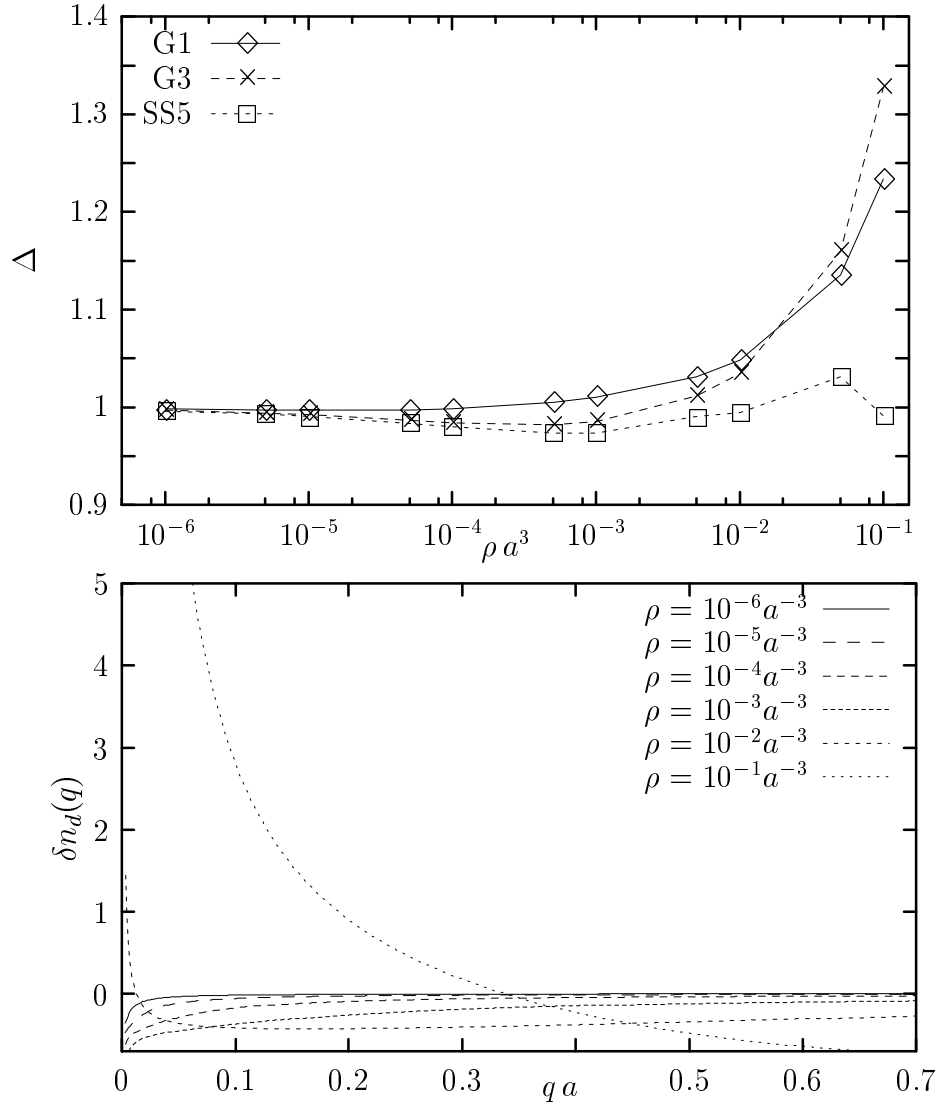


FIG. 9: Compressibility sum rule. Upper plot: The quantity  $\Delta$  of Eq. (76) is plotted as a function of the density for the potentials G1, G3 and SS5. Lower plot: Difference function of the momentum distribution with respect to that given for the exact sum rule at low  $q a$  at different densities for the SS5 potential.

self-consistent procedure, and that the resulting  $n_d(q)$  has indeed the required long wavelength behavior.

Calculations have been performed for five different pseudopotentials, three of the gaussian form, and two of the soft-sphere type, spanning a region of interaction range going from  $\sim 0.1r_0$  to  $\sim 10r_0$  and of strength  $a/r_0$  from  $\sim 0.02$  to  $\sim 0.8$ .

We found that IPC results for the energy per particle and the condensate fraction are in reasonably good agreement with the available DMC calculations, particularly for those potentials for which the scattering length  $a$  is closer to its value  $a_{\text{Born}}$  in Born approximation. In the limit of  $a/a_{\text{Born}} \rightarrow 1$  the low density expansion, Bogoliubov theory, DMC calculations and IPC model all give very close results. However, even for  $a/a_{\text{Born}} \sim 0.7$ , IPC provides a quite realistic representation of the cor-

responding Bose system.

We were also able to compute other interesting quantities, like the sound velocity, the chemical potential and the pairing function. The last quantity is directly related to the off-diagonal long range order in the gas, and to its superfluid properties at zero temperature. Therefore the IPC model appears to be an excellent candidate to study boson pairing in a quantitative way.

We also found that the range of validity of the low-density expansion is limited to  $\rho a^3 \sim 10^{-4}$ . Accordingly, for values of  $\rho a^3$  of the order or larger than  $10^{-3}$ , the results for the various quantities of interest do depend significantly on the shape of the potential and not only on the scattering length  $a$ .

The proposed theory can be easily extended to treat finite Bose systems, typical of trapped atomic vapours

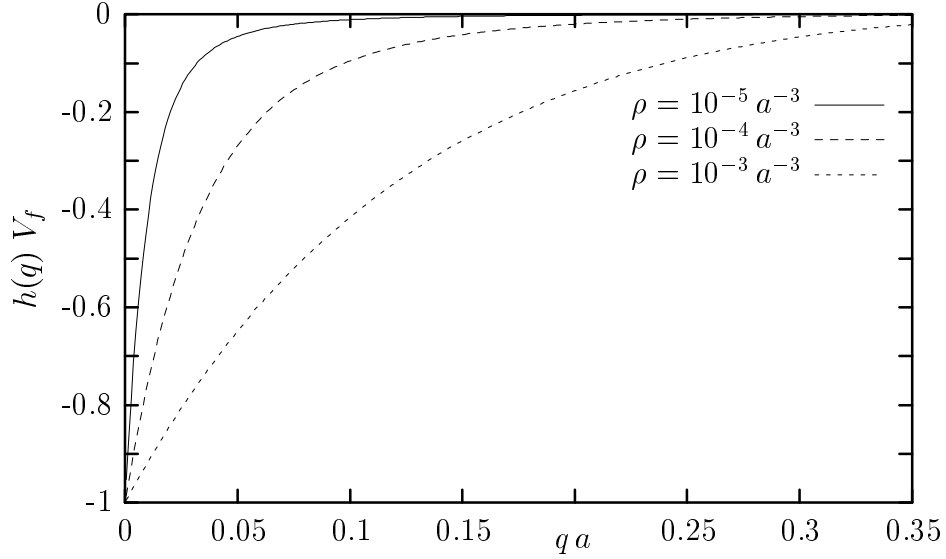


FIG. 10: Pair correlation function of the IPC model. The table displays the Fourier transforms of the pair correlation functions  $\tilde{h}(q)$  vertex corrected by  $V_f$ , obtained for the case of the potential SS10.

produced to study BEC and macroscopic coherent phenomena. Work in this direction is in progress.

The generalization to Fermi systems or to Fermi-Bose mixtures is also possible, although less straightforward. In this case, contrary to the Bose case, one has to deal with the elementary diagrams. In the Fermi case, the generic point of a cluster diagram can be reached by up to four bonds (instead of two), two of the  $h$ -type and two of the statistical type. This feature still guarantees a closed set of FHNC integral equations, but with kernels given by four-body functions.

A third, challenging perspective is the study of the excitation spectrum and of the superfluid properties. Such studies draw on the IPC physical picture of a number-conserving ground state with both a condensate and a coherent zero-momentum paired depletion; and on the HNC treatment developed in this paper, which allows for exact evaluation of the expectation value of a generic  $n$ -body operator.

### Acknowledgments

The authors are indebted to A. Fabrocini and J. Navarro for fruitful discussions. T.M.N. would like to thank the International School for Advanced Studies in Trieste for partial support during the completion of this work. The support from the grant MIUR-9902623127 (1999) is gratefully acknowledged by S.F. and A.S.

\*

### APPENDIX A

In this Appendix we derive the Euler equation resulting from the Ritz variational principle expressed by Eq. (50).

Let us compute the functional derivatives of the vertex corrections  $S_2$  and  $V_f$ . The vertex correction  $V_b$  can be expressed in terms of  $V_f$ .

$$\begin{aligned} \frac{\delta S_2}{\delta \tilde{h}(q)} &= C \frac{\delta V_f}{\delta \tilde{h}(q)} + \frac{q^2}{\pi^2 \rho} F(q), \\ \frac{\delta V_f}{\delta \tilde{h}(q)} &= -V_f^2 \left( \frac{\delta S_2}{\delta \tilde{h}(q)} + \frac{2\tilde{h}_0}{(1 - \tilde{h}_0 V_f)^3} \frac{\delta V_f}{\delta \tilde{h}(q)} \right), \end{aligned} \quad (A1)$$

with

$$\begin{aligned} C &= \int \frac{d\vec{k}}{(2\pi)^3 \rho} \frac{\tilde{h}^2(k)(1 + \tilde{h}^2(k)V_f^2)}{(1 - \tilde{h}^2(k)V_f^2)^2}, \\ F(q) &= \frac{\tilde{h}(q)V_f}{(1 - \tilde{h}^2(k)V_f^2)^2}. \end{aligned} \quad (A2)$$

The solution of the above linear system is given by

$$\begin{aligned} \frac{\delta S_2}{\delta \tilde{h}(q)} &= \frac{q^2}{\pi^2 \rho} \left( \frac{a_1}{a_1 + C} \right) F(q), \\ \frac{\delta V_f}{\delta \tilde{h}(q)} &= -\frac{q^2}{\pi^2 \rho} \left( \frac{1}{a_1 + C} \right) F(q), \\ a_1 &= \frac{2\tilde{h}_0}{(1 - \tilde{h}_0 V_f)^3} + \frac{1}{V_f^2}. \end{aligned} \quad (A3)$$

The functional variation of the expectation value of the kinetic energy results to be

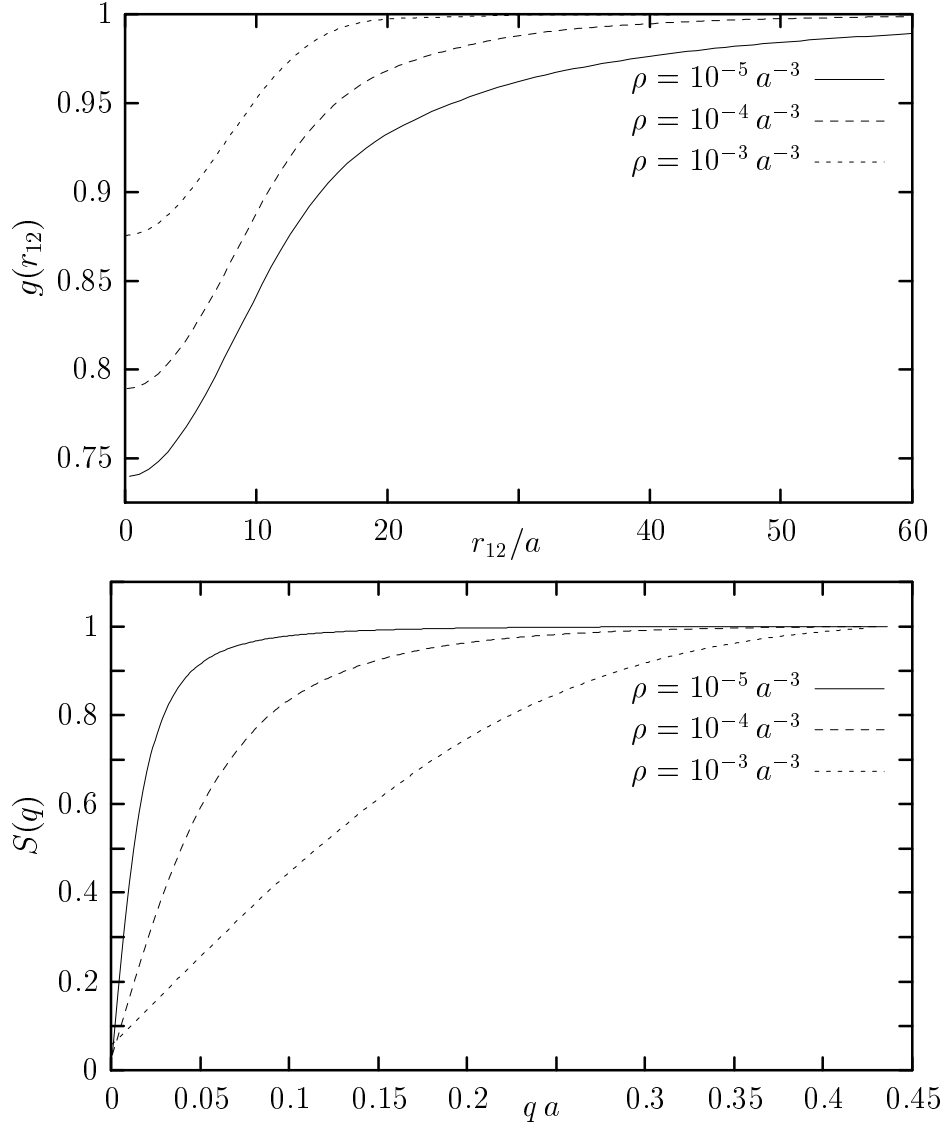


FIG. 11: Upper plot: Two-body distribution function  $g(r_{12})$  of the IPC model of a Bose gas interacting with the potential SS10. Lower plot: the same for the static structure factor  $S(q)$ .

$$\begin{aligned} \frac{\delta \langle T \rangle}{\delta \tilde{h}(q)} &= \left( \frac{q^2}{\pi^2 \rho} \right) \frac{\hbar^2}{2m} V_f q^2 F(q) \\ &+ \frac{\delta V_f}{\delta \tilde{h}(q)} \left( 2 \frac{\langle T \rangle}{V_f} + \frac{\hbar^2}{m} \int \frac{d\vec{k}}{(2\pi)^3 \rho} \frac{k^2 \tilde{h}^4(k) V_f^3}{(1 - \tilde{h}^2(k) V_f^2)^2} \right), \end{aligned} \quad (\text{A4})$$

which leads to

$$\begin{aligned} \frac{\delta \langle T \rangle}{\delta \tilde{h}(q)} &= \left( \frac{q^2 V_f}{\pi^2 \rho} \right) \frac{\hbar^2}{2m} (q^2 F(q) - 2F(q) T_1), \\ T_1 &= \frac{1}{a_1 + C} \int \frac{d\vec{k}}{(2\pi)^3 \rho} \frac{k^2 \tilde{h}^2(k)}{(1 - \tilde{h}^2(k) V_f^2)^2}. \end{aligned} \quad (\text{A5})$$

The functional variation of the potential energy expectation value  $\langle V \rangle$  is given by

$$\frac{\delta \langle V \rangle}{\delta \tilde{h}(q)} = \left( \frac{q^2 V_f}{\pi^2 \rho} \right) F(q) \left( \frac{\tilde{V}_b(q)}{\tilde{h}(q)} + \tilde{V}_a(q) - V_1 \right), \quad (\text{A6})$$

where  $\tilde{V}_a(q)$  and  $\tilde{V}_b(q)$  are defined as

$$\begin{aligned} \tilde{V}_a(q) &= \left( \tilde{v} \left| \frac{\tilde{h}^2 V_f^2}{1 - \tilde{h}^2 V_f^2} \right|_q \right), \\ \tilde{V}_b(q) &= \frac{1}{2} \left( \frac{(1 + \tilde{h}(q) V_f)^2}{(1 - \tilde{h}_0 V_f)^2} \tilde{v}(q) \right. \\ &\quad \left. + (1 + \tilde{h}^2(q) V_f^2) \left( \tilde{v} \left| \frac{\tilde{h}}{1 - \tilde{h}^2 V_f^2} \right|_q \right) \right), \end{aligned} \quad (\text{A7})$$

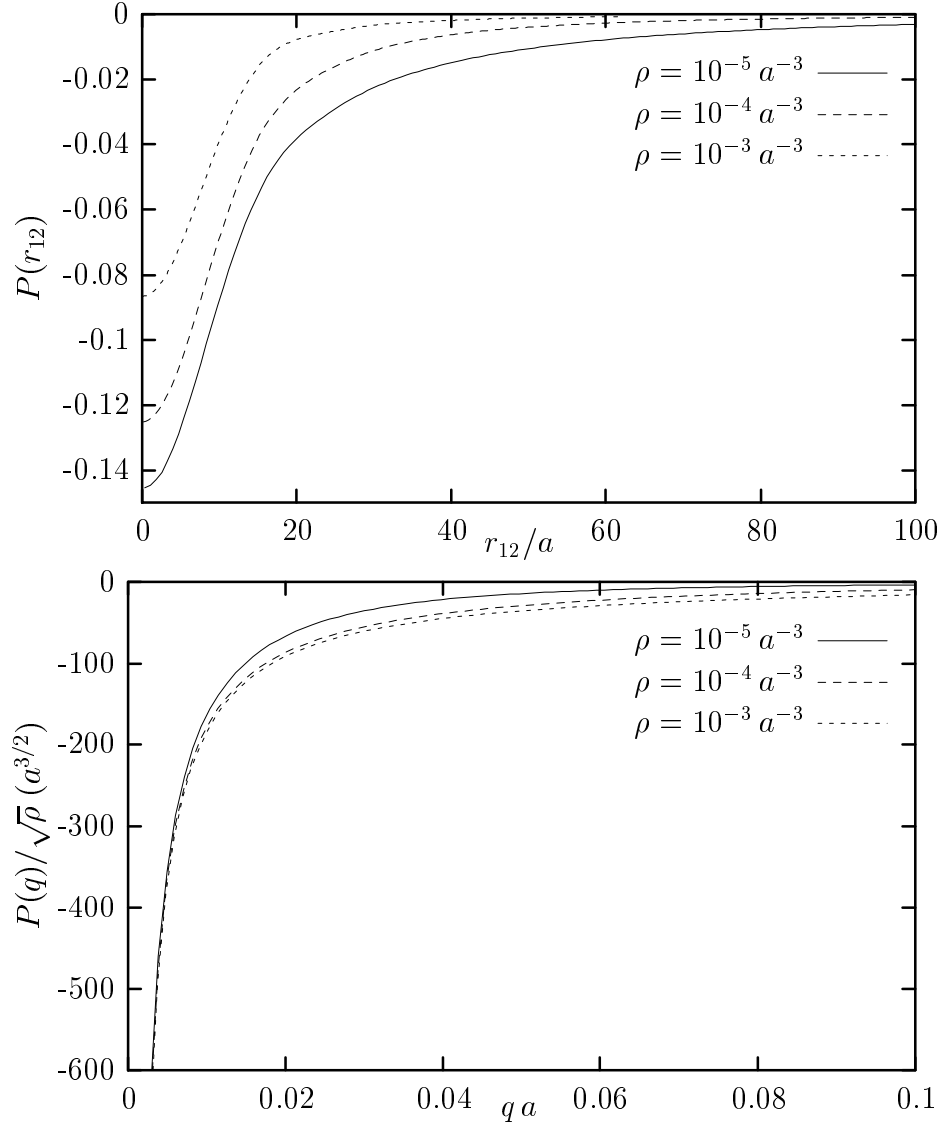


FIG. 12: Upper plot: Pairing function  $P(r_{12})$  of the IPC model of a Bose gas interacting with the potential SS10. Lower plot: the same for the pairing function in momentum,  $\tilde{P}(q)$ , space divided by  $\sqrt{\rho}$  to fit the scale.

and the constant term  $V_1$  by

$$\begin{aligned}
 V_1 = & \frac{1}{a_1 + C} \left( \frac{1 + \tilde{h}_0 V_f}{(1 - \tilde{h}_0 V_f)^3} \int \frac{d\vec{k}}{(2\pi)^3 \rho} \frac{\tilde{h}(k) \tilde{v}(k)}{1 - \tilde{h}(k) V_f} \right. \\
 & + \frac{1}{(1 - \tilde{h}_0 V_f)^2} \int \frac{d\vec{k}}{(2\pi)^3 \rho} \frac{\tilde{h}(k) \tilde{v}(k)}{(1 - \tilde{h}(k) V_f)^2} \\
 & + 2 \int \frac{d\vec{k}}{(2\pi)^3 \rho} \tilde{v}(k) \left( \frac{\tilde{h}^2}{(1 - \tilde{h}^2 V_f^2)^2} \Big| \frac{\tilde{h}^2 V_f^2}{1 - \tilde{h}^2 V_f^2} \right)_k \\
 & \left. + \int \frac{d\vec{k}}{(2\pi)^3 \rho} \tilde{v}(k) \left( \frac{\tilde{h}(1 + \tilde{h}^2 V_f^2)}{(1 - \tilde{h}^2 V_f^2)^2} \Big| \frac{\tilde{h}}{1 - \tilde{h}^2 V_f^2} \right)_k \right) .
 \end{aligned}$$

We can now write down explicitly the Euler equation resulting from Eq. (50)

$$F(q) \left( \frac{\hbar^2}{2m} (q^2 - 2T_1) + \frac{\tilde{V}_b(q)}{\tilde{h}(q)} + \tilde{V}_a(q) - V_1 \right) = 0 . \quad (\text{A8})$$

Since  $F(q)$  cannot be equal to zero, then the Euler equation becomes

$$\frac{\hbar^2}{2m} q^2 \tilde{h}(q) + (\tilde{V}_a(q) - \lambda) \tilde{h}(q) + \tilde{V}_b(q) = 0 , \quad (\text{A9})$$

with

$$\lambda = \frac{\hbar^2}{m} T_1 + V_1 . \quad (\text{A10})$$

The quantities  $\tilde{V}_a(q)$ ,  $\tilde{V}_b(q)$  and  $\lambda$  all depend on  $h(r)$  in a highly non linear way. Therefore eqs.(A9) and (A10) need to be solved by means of a self consistent iterative

procedure. The equation (A9) is equivalent to Eq. (60), as one can verify by expressing  $\tilde{h}(q)$  in terms of  $n_d(q)$ .

- 
- [1] M. Anderson, *et al.* Science **269**, 198 (1995); C. C. Bradley, *et al.* Phys. Rev. Lett. **75**, 1687 (1995); K. B. Davis, *et al. ibid.* **75**, 3969 (1995); M. O. Mewes, *et al. ibid.* **77**, 416 (1996);
  - [2] F. Dalfovo, *et al.* Rev. Mod. Phys. **71**, 463 (1999).
  - [3] W. Ketterle, D. S. Durfee, and D. M. Stamper-Kurn, in *Bose-Einstein Condensation in Atomic Gases*, Proceedings of the International School of Physics "Enrico Fermi", Course CXL, edited by M. Inguscio, S. Stringari, and C. Wieman, (IOS Press, Amsterdam, 1999).
  - [4] A. J. Leggett, Rev. Mod. Phys. **73**, 307 (2001).
  - [5] N. N. Bogoliubov, J. Phys. (USSR) **11**, 23 (1947); reprinted in D. Pines, *The Many Body Problem* (Benjamin, New York, 1962).
  - [6] K. Huang, *Statistical Mechanics*, (John Wiley & Sons, New York, 1987).
  - [7] E. Feenberg, *Theory of Quantum Fluids*, (Academic Press, New York, 1969).
  - [8] M. D. Girardeau, and R. Arnowit, Phys. Rev. **113**, 755 (1959).
  - [9] J. G. Valatin and D. Butler, Nuovo Cimento **10**, 37 (1958).
  - [10] W. A. B. Evans, and Y. Imry, Nuovo Cimento B **63**, 155 (1969).
  - [11] S. R. Shenoy, and A. C. Biswas, J. of Low Temp. Phys. **28**, 191 (1977).
  - [12] D. Bohm, B. Salt, Rev. Mod. Phys. **39**, 894 (1967).
  - [13] N. M. Hugenholtz, and D. Pines, Phys. Rev. **116**, 489 (1959).
  - [14] D. G. Henshaw and A. D. B. Woods, Phys. Rev. **121**, 1266 (1961).
  - [15] P. Nozières, D. Pines, *The Theory of Quantum Liquids* (Perseus Books Publishing, L. L. C., 1999)
  - [16] C. W. Gardiner, Phys. Rev. A **56**, 1414 (1997).
  - [17] A. J. Leggett in *Modern trends in the Theory of Condensed Matter*, edited by A. Pekolski and R. Przystowa, (Springer Verlag, Berlin 1980); J. Phys. (Paris) Colloq. **41**, 456 (1969).
  - [18] M. Randeria in *Bose-Einstein Condensation*, edited by E. Griffin, D. W. Snoke and S. Stringari, (Cambridge University Press, Cambridge, 1995).
  - [19] J. M. Blatt, *Theory of superconductivity*, (Academic, New York, 1964).
  - [20] J. Gavoret, and P. Nozières, Ann. of Phys. **28** 349 (1964) 349; L. Reatto and G. V. Chester, Phys. Rev. **155**, 88 (1967).
  - [21] S. Stringari, in *Bose-Einstein Condensation*, edited by E. Griffin, D. W. Snoke and S. Stringari, (Cambridge University Press, Cambridge 1995).
  - [22] S. Fantoni, and S. Rosati, Nuovo Cimento A **20** 179 (1974).
  - [23] S. Fantoni, and A. Fabrocini, in *Microscopic quantum-many body theories and their applications*, Lecture Notes in Physics, Vol. **510**, edited by J. Navarro and A. Polls, (Springer-Verlag, Berlin, 1998).
  - [24] J. Navarro, in *Advances in Quantum Many-Body Theory*, edited by A. Fabrocini, S. Fantoni and E. Krotscheck, World Scientific, in press.
  - [25] J. Navarro, private communication.
  - [26] C. H. Aldrich III, and D. Pines, J. of Low Temp. Phys. **25**, 677 (1976).
  - [27] S. Moroni, S. Fantoni, G. Senatore, Phys. Rev. B **52**, 13547 (1995).
  - [28] S. Fantoni, Nuovo Cimento A **44**, 191 (1978).
  - [29] V. R. Pandharipande, Nucl. Phys. A **174**, 641 (1971) 641; *ibid.* **178**, 123 (1971); V. R. Pandharipande and H. A. Bethe, Phys. Rev. C **7**, 1312 (1973).
  - [30] M. L. Ristig, Nucl. Phys. A **317**, 163 (1979).
  - [31] M. L. Ristig, and P. M. Lam, J. of Low Temp. Phys. **40**, 571 (1980).
  - [32] S. Fantoni, Nucl. Phys. A **363** 381 (1981).
  - [33] G. Baym, in *Mathematical Methods Solid State and Superfluid Theory*, edited by R. C. Clark, G. H. Derrick, (Oliver & Boyd, Edimburgh, 1969).
  - [34] T. D. Lee and C. N. Yang, Phys. Rev. **105**, 1119 (1957); T. D. Lee, K. Huang and C. N. Yang, Phys. Rev. **106**, 1135 (1957).
  - [35] S. L. Cornish, *et al.*, Phys. Rev. Lett. **85**, 1795 (2000).
  - [36] S. Cowell, *et al.*, e-print cond-mat/0106628.
  - [37] S. Giorgini, J. Boronat, and J. Casulleras, Phys. Rev. A **60**, 5129 (1999).
  - [38] C. J. Joachain, *Quantum collision theory*, (North Holland, Amsterdam, 1979).
  - [39] E. H. Lieb, and J. Yngvason, Phys. Rev. Lett. **80** 2504 (1998). E. H. Lieb, R. Seiringer, and J. Yngvason, Phys. Rev A **61**, 043602 (2000).
  - [40] A. Fabrocini and A. Polls, Phys. Rev. A **60** 2319 (1999); **64**, 063610 (2001)
  - [41] T. T. Wu, Phys. Rev. **115** 1930 (1959).
  - [42] S. T. Beliaev, JETP **34**, 433 (1958).
  - [43] M. L. Ristig and J. W. Clark, Phys. Rev. B **40**, 4355 (1989).
  - [44] S. R. Shenoy, A. Sarsa, T. M. Nguyen and S. Fantoni, in preparation.
  - [45] For the Jastrow model the HNC cluster decomposition coincides with the Mayer expansion.
  - [46] Notice that the actual integrations in  $I$  lead to a factor  $\Omega$  for each cluster integral, because of the translational invariance of the cluster integrands.
  - [47] Notice that, in calculating the normalization intergral of Eq. (4), the  $1/N$  terms give a finite contribution.
  - [48] the topological factor  $t_T$  is given by the inverse of the number of labels permutations which maintain the same topological structure of  $\Gamma$  [23]